REMARKS

Examiner's Objections to the Drawings; Amendments to the Specification:

Examiner has objected to the drawings under 37 CFR 1.83(a) as not showing every feature of the invention specified in the claims. In response thereto, Applicant respectfully directs Examiner's attention to the new drawing sheet submitted herewith. Applicant respectfully believes that the newly submitted drawing addresses Examiner's basis of the objection under 37 CFR 1.83(a) and, accordingly, requests Examiner's approval of same. However, should Applicant's drawing not be fully responsive to Examiner's objections and requirements, then Applicant respectfully requests a non-final opportunity to correct same. Applicant further submits that the specification has now been amended, as detailed hereinabove, to appropriately reference and described Applicant's new drawing. Applicant notes that no new matter has been presented in either the drawing or amendments.

Examiner's Objections & Rejections to the Specification & Claims; Applicant's Responses:

Examiner has objected to the specification under 35 USC 112, first paragraph; and, has rejected elected Claims 1-10, 13, 14, 89, and 91-95 under 35 USC 112, first paragraph; 35 USC 101; 35 USC 112, second paragraph; 35 USC 103(a); and, 35 U.S.C. 102(b), citing a multitude of published articles and a series of patent references in support of Examiner's various arguments asserting that there is no reputable evidence of record to support any allegations or claims of invention made by Applicant, and that Applicant's invention is based on the concept of cold fusion. (Although Examiner has raised many additional related arguments, for purposes of brevity Applicant will not reiterate same, but will rather draw reference to general arguments reiterated by Examiner throughout Examiner's nearly fifty (50) page Office Action.)

In response to Examiner's arguments, and with all due respect to Examiner, Applicant respectfully submits that Examiner has largely misread, misrepresented, and misunderstood Applicant's invention, both in the specification and in the claimed subject matter. Indeed, although Applicant believes that Examiner has provided a lengthy and thoughtful response, Examiner's response is highly prejudicial and, for the most part, inaccurately represents the scope and nature of Applicants proffered technological and inventive advances.

To begin, Examiner has given a lengthy history of cold fusion and the position of the scientific community in response thereto. <u>Unfortunately, Examiner has improperly and inaccurately categorized Applicant's invention as that of a cold fusion process.</u> Quite to contrary, however, **Applicant's invention is a variant of hot fusion** - a very different process from cold fusion, and recognized in the scientific community. For example, when electrons in a TV picture tube impact the screen exciting phosphors to produce light, one may touch the screen without burning one's hand, yet every competent physicist can calculate that the kinetic temperature of such electrons exceeds ten million degrees Centigrade. <u>Applicant's invention is not a cold fusion process, nor was it ever claimed to be such a process.</u> Applicant addressed the cold fusion process in his application merely to provide a historical synopsis of the **various** fusion reaction efforts (this is supported by the fact that Applicant presents the cold fusion description in the "Background of the Invention" section of the patent application - the same section from which Examiner draws support for his rejections). <u>However, Applicant has not stated or claimed anywhere in his patent application that his invention is one of cold fusion, nor has Examiner been able to cite to any such claim made by Applicant.</u>

Instead, <u>based solely on a single paragraph</u> contained on pages 7-8 of Applicant's "Background of the Invention" section (many more pages of which contain far more paragraphs describing fusion reactions **unrelated** to cold fusion), Examiner has elected to classify, much to the detriment and prejudice of Applicant, the instant invention as one of cold fusion, and has thus provided Applicant with an Office Action entirely based on such unfounded assertions. Additionally, the numerous references cited by Examiner, although applicable to cold fusion processes, are wholly unrelated and inapplicable to Applicant's fusion process. Applicant cannot accurately and properly respond to an action comprising seemingly endless arguments rejecting an invention that Applicant has not described or claimed as being one of his own.

Scope and Nature of Applicant's Invention; Examiner's Cited References:

As described in Applicant's originally filed application, in conventional hot deuterium fusion, the means for overcoming the Coulombic repulsion of two fusing nuclei is to provide one nucleus with a sufficient kinetic velocity with respect to the other. When the two nuclei are a critical distance apart, such distance being a function of their atomic number and atomic mass, the strong nuclear force dominates over the Coulombic repulsion and the nuclei fuse. Applicant's invention presents a method whereby a large surface charge on a conducting lattice effectively shields the positive charge of the one nucleus against the positive charge of the other so that a lower kinetic velocity is required to achieve the critical distance. Lower kinetic velocity translates to lower mean temperature.

In cold fusion cells, the basic premise is that the unaltered intrinsic electron density of the metallic lattice provides this electronic shielding. With this limitation, cold fusion does not work, as is noted by Examiner, and as is referenced in the majority of papers provided by Examiner. However, one of the keys to Applicant's invention is a technique for significantly

enhancing the electronic shielding – a technology and methodology absent from all of the patents and papers referenced by Examiner. As an analogy, the late-1800 car manufacturers did have an internal combustion engine. However, it was not until the weight-to-horsepower ratio of the engine was significantly decreased that the Wright brothers were able to use it to power their first airplane. That is, many fundamental inventions rely on known mechanical models that are optimized and better than those available in the past, crossing an operational threshold that makes the invention possible. Such is the case of Applicant's invention.

Examiner references 14 patents and 107 non-patent documents. In general, the non-patent documents concern cold fusion, the basic premise of which Applicant already rejects. A year ago one may have made the argument that thermonuclear fusion "on a desktop" was a fantasy, but verified results from UCLA have refuted this argument (*see* Exhibit A). Clearly, fusion is slowly being removed from the fission thermonuclear bottle.

As noted above, the quality of the shielding obtainable makes Applicant's invention possible. Such electron densities required can only be obtained through a charge concentrator with a precisely defined tip in the nanoscale. Just as the existence of macroscopic projections and protuberances on the electrodes are insufficient, so too will the Wright brothers' airplane not fly with an overweight and underpowered 1880 IC engine.

Accordingly, recognizing the need for nanofabrication, one can dismiss all previous patents before about 1996, as such techniques were not available. The only patent referenced by Examiner after 1996 is U.S. Patent No. 6,489,704, which discloses a thermionic energy converter with fractional surface contacts, and whose technology and claims bear no relevance to the present invention.

Although Applicant has made his election of the claims, Applicant respectfully notes that Examiner has not recognized the common features in all of the groups of claims enumerated; that is, of a specialty surface generating sufficiently high charge density on the surface protuberances to allow significantly lower kinetic temperatures for hydrogen and its isotopes to nuclear fuse. This feature is described in the example given in Applicant's specification on page 23. The active portion or tips of the protuberances of Applicant's reacting surface are within tens of nanometers and, thus, are atomically sharp.

Indeed, and contrary to Examiner's assertions, the manufacture of a nano-protuberance surface may be done, and has been done, by many known methods. In particular, scientists have constructed single protuberance structures to the single atom level, and have used them extensively in the tips of atomic scanning and probe microscopes. Applicant encloses herewith, for Examiner's reference, a report that Applicant has written describing such devices (*see* Exhibit B). Applicant further notes that there are companies commercially producing the atomically flat surface needed for fabrication – Applicant submits herewith literature from one such company (see Exhibit C). In further support of such nano-fabrication, Applicant submits an article showing a method for nanofabrication of a two dimensional array (*see* Exhibit D). Still further, there are numerous other methods in use for array fabrication (*see* Exhibit E, Fig. 2), including the techniques of nanolithography, and strain-induced pattern formation. Applicant encloses another article illustrating the growth of whiskers on a nanoscale (*see* Exhibit F). Applicant notes that the materials science literature in the last 7 years is replete with examples of such techniques of nanofabrication; these techniques are widely published and indeed known to the scientific community. In further support of such known technology, Applicant submits herewith a detailed engineering analysis completed to calculate the electric field and charge density on an

optimized cone separated from an electrically neutral flat plate, illustrating a practical construction rather than the optimized construction (zero separation distance) noted in the patent specification (*see* Exhibit G).

On page 8 of Examiner's Office Action, Examiner refutes Applicant's total invention and takes no note of the theory presented in Applicant's specification. Examiner extensively quotes "accepted theory" without specifying how the snippet of theory presented varies from it. Applicant submits that the application is not intended to present a learned thesis on quantum mechanics. However, in the interest of explaining Applicant's Equations 1-3, Applicant encloses a small section on basic physics of the Bohr radius, indicating how the muon binding energy is calculated (*see* Exhibit H). From this expression for Bohr radius, clearly forcing the equality of a Bohr radius of increasing mass "m" and charge "Z" yields:

$$A_Z = h^2/(kZ^2e^2m_e) = A_{muon} = h^2/(ke^2m_{muon}) \text{ } so \text{ } that \text{ } Z^2m_e = m_{muon}, \text{ } as \text{ } noted.$$

Applicant's equation considers an equivalent Z if all electrons were placed in a single energy shell. Although this violates the Pauli exclusion principle if the electrons are bound to the ion, it is quite different if the electrons are attached to the atomic metallic lattice on the surface of the cone, and the deuterium ion comes arbitrarily near this electron concentration. In this case, the solution of the Schroedinger equation for bound electrons on the deuterium ion nucleus does not apply.

Examiner further objects to the form of Applicant's Equation 3 on multiple grounds, not the least of which is that the undetermined constants are not specified a priori. In response to Examiner's objection, Applicant submits herewith an interesting paper from The Astrophysics

Journal that looks at Thermonuclear Fusion and screening, and notes the fusion-enhancement factor due to screening in the solar plasma (*see* Exhibit I).

Applicant notes that Equation 3 does not have a rigorous derivation, but stems from an observation that absent muon data, there is a reasonable straight-line correspondence between the logarithm of fusion temperature and the number of nucleon interactions for single proton fusion. The mathematical model is extended with the addition of the equivalent shielding created by the muon, and its corresponding fusion temperature. The coefficients are fit to the data by least squares, a rigorous mathematical method, which will yield only one solution (contrary to Examiner's assertions). All mathematical models of physical events must make assumptions to remain finite. The objective is to make the minimum number of assumptions so that the model may reasonably predict future behavior.

Examiner further quotes Lindley who describes the electron cloud model in a metal with respect to elevation of mean electron mass. Such derivations of elevated electron masses more properly belong in BCS superconductor theory than in normal metals. No claim is made by Applicant that the electrons on the cone tip detach to the deuterium ions. Indeed, the entire concept of electron tunneling, used in numerous other inventions, relies upon the quantum mechanical uncertainty of the electron's exact position. Thus, many electrons may momentarily be arbitrarily close to the deuterium nuclei. Fukai is correct; deuterium nuclei in an unaltered palladium lattice cannot come close enough for fusion at low temperatures. However, this invention describes a highly enhanced surface charge density than that encountered in the unaltered metallic lattice alone. Like the Wright brother's IC engine, the enhanced charge density allows the fusion process.

Examiner further indicates that Applicant has provided inadequate disclosure of how Applicant's cones or wedges of the reacting surface can be manufactured – despite the fact that Applicant has already stated in the application that such manufacture may be had via nanotechnology. As discussed hereinabove, and as evidenced in the attached literature of the Exhibits, many known nanotechnology methods may be utilized to manufacture Applicant's invention. Applicant notes the recent textbooks of such methods, as referenced in Applicant's Exhibit B. Regarding electroplating, one of the primary mechanisms of failure of lead acid batteries is the growth of dendrites in the nanoscale between anode and cathode in the electrolyte. This growth has been studied for many years and its science is well developed. Further, there are multiple techniques in materials nanoscience including Atomic Layer Deposition (ALS) that can be utilized to provide precise and repeatable placement of atomic layers on surfaces.

Applicant's Claim Amendments:

To better clarify Applicant's invention, Applicant has now amended certain Independent Claims to reflect that each protuberance/cone/wedge of Applicant's reacting surface comprises an "atomically sharp apex." Applicant respectfully submits that the cited references and prior art do not teach or fairly suggest Applicant's invention as now claimed. In view of the foregoing arguments and evidence, reconsideration is respectfully requested.

CONCLUSION

The above-made amendments are to form only and thus, no new matter was added. Applicant respectfully believes the above-made amendments now place the Claims and application in condition for allowance. Should there be any questions or concerns, the Examiner is invited to telephone Applicant's undersigned attorney.

Respectfully submitted,

Dated: September 27ᵗʰ, 2005

Ashish D. Patel
Attorney for Applicant
Reg. No. 50,177

Myers & Kaplan
Intellectual Property Law, L.L.C.
1899 Powers Ferry Road
Suite 310
Atlanta, GA 30339
Phone: 770-541-7444
Fax: 770-541-7448

IN THE UNITED STATES PATENT AND TRADEMARK OFFICE

In re:	Robert Indech	)	Docket No:	23050-RA
		)		
Serial No.:	10/735,406	)	Examiner:	Behrend, Harvey E.
		)		
Filed:	December 12, 2003	)	Group Art:	3641

For: APPARATUS AND METHOD FOR FACILITATING NUCLEAR FUSION

RESPONSE TO OFFICE ACTION OF JULY 19, 2005

EXHIBIT B

Design and Construction of Probe Tips for Scanning Tunneling Microscopy (STM)

Robert Indech

Design and Construction of Probe Tips for Scanning Tunneling Microscopy (STM)

Abstract

Unique visualization of the true atomic surface structure is made possible by the geometric scanning and resolution of the scanning tunneling microscope (STM). In this device, an atomically sharp tip is maneuvered over the object of interest, with a potential being applied between it and the object. Instantaneous measurement of current in this circuit can be computer resolved into a simulated surface image. In practical design, the quantum electronic states of these tips are critical to their operation. This paper will review the literature on the theory of such tips in STM, and discuss considerations in their construction. A possible solution utilizing nanotechnological construction technique for problems encountered in their use will be presented.

I. Introduction

Unique visualization of the true atomic surface structure is made possible by geometric scanning and computer image reconstruction of the scanning tunneling microscope. The theory of scanning tunneling microscopy (STM) is reviewed quite well in Chapter 6 of the Woodruff and Delchar Text, <u>Modern Techniques of Surface Science – Second Edition</u>[1]. In brief, an atomically sharp tip is constructed and is controllably maneuvered over the object of interest, a potential being applied between the probe tip and the tip and the surface of the object. As a result of the electrical potential, a current is generated, the magnitude of which is a function of the separation distance from the tip to the surface and other factors. The exact position of the tip is controlled by the application of electrical potentials to mutually orthogonal

piezoelectric elements attached to the tip. The mechanical configuration is shown in Figure 1, indicating
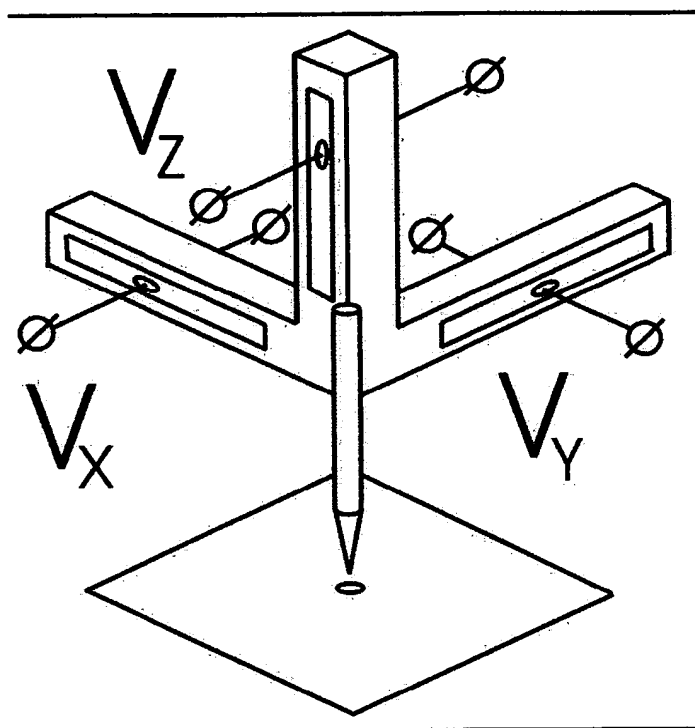
the tip and piezoelements.

Figure 1. Basic Configuration of the Scanning Tunneling Microscope

(taken from Figure 1 of Reference 2, Frantsesson and Zuev)

In operation, the tip potential is kept low to prevent ion generation as is used in filed emission

microscopy. The tip characteristics are critical, as the interaction of atomic orbital wave functions of the

tip and the object surface determine the exact conductance. Thus, the exact material of the tip as well as

its physical geometry with microscope operation must be considered.

II. Quantum Theory Considerations

The tunneling current, I, is proportional to the exponent ε raised to the power $-2KD$, as in Equation II.1 where D is the effective distance between the tip and the object surface and K is the characteristic exponential inverse decay length.

Eq. II.1 $\quad I = C_1 \cdot \varepsilon^{-2KD} \quad$ where $\quad K = \dfrac{\sqrt{2m\phi}}{h}$

where m is the electron mass, h is Planck's constant and ϕ is the effective local work function.[1]

As there is some uncertainty in D and ϕ, scientists have contemplated numerous models to remove the specific properties of the tip from the problem. In early work, Tersoff and Hamann considered the "s-wave model" in which the conductance is proportional to the local density of states $\rho(r_t, E_F)$, as given in Equation II.2.

Eq. II.2 $\quad \rho(r_t, E_F) = \Sigma |\varphi_v(r)| \delta(E_V - E) \Leftrightarrow r = r_t, E = E_F$

where φ is the electronic wavefunction at the tip, E is the energy, and r is the position coordinate, taken at r_t, the tip position.[3] In this model, the tip current maps out a contour of the constant values of the local density of states with the Energy E taken at the Fermi Energy level, E_F. Unfortunately, this model yields resolutions no better than 6-9 Angstroms.

A better model considers the P and D electron orbital states of the metal tips. This theory, advanced by Chen in 1990, yields substantially better resolution at a larger tip to sample distance.[4] However, to gain this resolution requires specific tip materials such as the D-band transition metals such as tungsten, platinum and iridium or certain semiconductor like silicon which form P_z-like metallic dangling bonds.

III. Tip Fabrication

.   By the Chen model, there are limitations as to the specific materials that can be used for the tips. Further, one must consider the method of manufacture of such tips. In the design of field ionization microscope tips one desires a nearly hemispherical and atomically smooth tip surface. One method of such construction is the application of a sufficiently high electric field to the rough tip, which blasts any protrusions from the tip as positive emitted ions. Solution of Maxwell's equations in the static regime in the region around the sharply pointed tip indicates a major charge concentration effect. As nature tends always to smooth out irregularities, then a smooth hemispherical surface will be created. However, this result is not appropriate for the resolution desired in the STM.

Aeshimann et al describes a process of creation of silicon oxide tips, as shown in Figure 2. These tips, utilized for scanning near-field optical microscopy utilize 12-micron silicon oxide tips integrated over the end of a silicon cantilever.[5] Essential to this design is repetitive micro machining to yield tip geometry.
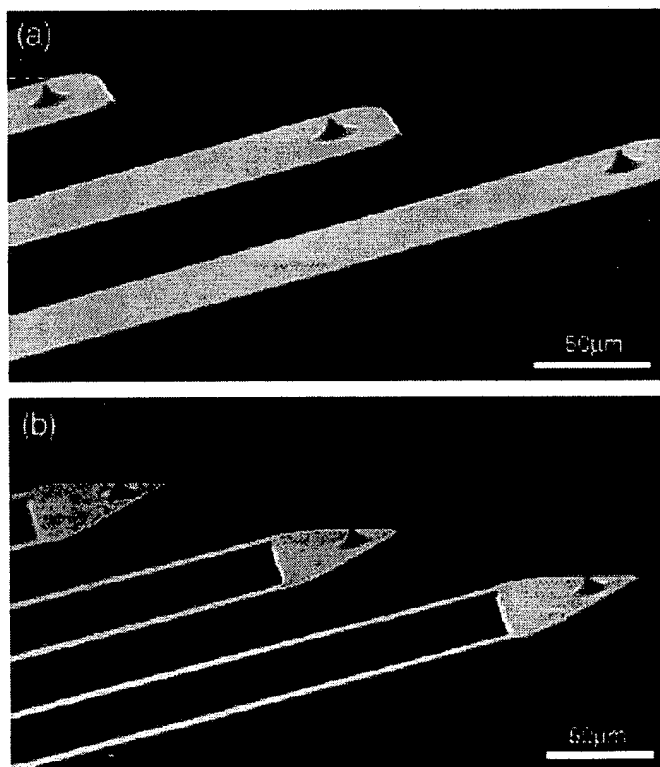

Figure 2. Silicon-dioxide tips (taken from Figure 1 of Reference 5, Aeshimann et al)

As noted by Liu and Gamble, desirable properties for the scanning probe microscope tips include 1) good tip sharpness with small tip radius 2) small force constant and 3) high resonant frequency.[6] In their process, the sharp tips are formed by oxidation sharpening rather than direct anisotropic etching (AE). In AE, a photolithographically patterned region of silicon dioxide forms on an epitaxial silicon layer that is then immersed in ethylene diamine pyrocathechol (EDP) producing pyramid shaped tips. The authors note that while this process, AE, may produce atomically sharp tips, it is difficult to control due to variations in process parameters. The authors improve the general process by serial growth of thermal oxide on the tip unit and subsequent removal, in a non-uniform way, of the oxide using dilute hydrofluoric acid. By this subtractive process, the apex becomes sharper after each sharpening cycle.

A favored technique for tip fabrication involves plasma etching and oxidation sharpening, as reviewed by Tabib-Azar and Wang, and is shown in Figure 3. In their process, the starting substrate is a double-side-polished silicon on insulator (SOI) wafer with a 15-uM device layer, a 1-uM buried oxide layer and a 400-uM handle layer. After cleaning the wafer has a thermally oxidized 1-uM silicon dioxide layer grown which is photolithographically fashioned into defined circular patterns. The exposed thermal oxide is etched by buffered hydrofluoric acid and then silicon fluoride plasma etchings produces conical silicon tips, as shown in Figure 3A. Conventional thermal oxidation sharpening produces a peak as shown in Figure 3B, with a 50 Angstrom radius. Finally, in their process, a coaxial shielding layer is built up around the tip, as shown in Figure 3C, for better STM electrical performance.[7]
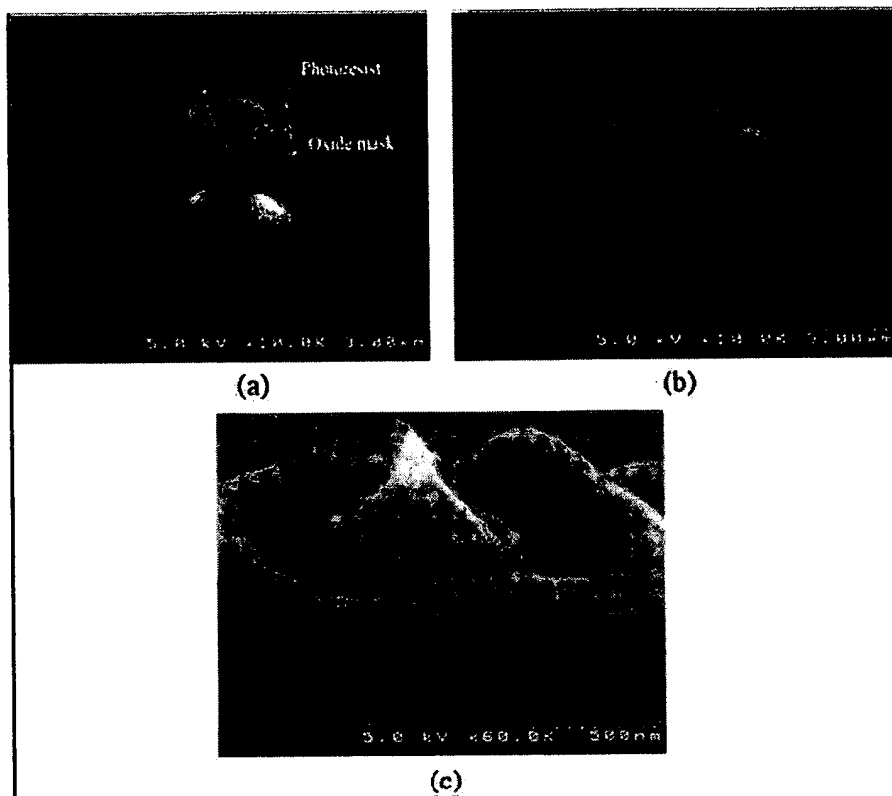
(a) (b)

(c)

Figure 3. Tip SEMS (taken from Figure 8 of Reference 7, Tabib-Azar and Wang)

In a more advanced fabrication methodology, Cruchon-Dupeyrat et al utilizes CAD design techniques and automated vector scanning to do the nanofabrication of the tip[8]. In their process, a multi-mode scanning probe microscope (SPM) is linked with a computer control for precise automated control of the SPM tip. This arrangement allows almost molecule-by-molecule fabrication of the new tip or indeed any desired nanostructures. While offering unprecedented control, it suffers from the constant defect of all devices of this class, that is, the excessive time required for complete fabrication before contamination sets in, even under ultra high vacuum conditions. It would be preferable to use nanotechnology self-assembly methods rather than atom be atom placement.

IV. Problems in Current Production Methods

At present, probe tips are constructed on a one by one basis. Built up over a conventional substrate, they experience constant contamination and, with loss of sharpness and concurrent degradation of STM performance, a need for replacement. Further, there is difficulty in cleaning the tips, a process to remove secondary adhered species without losing the atomic sharpness. Conventional fabrication is a subtractive process, with etching cycles. Simply applying a high potential to "blast-off" secondary adherents would work only if the exact tip geometry were known and uniform so that the applied potential could be kept low enough to prohibit loss of the metallic tip atoms themselves. Unfortunately, variation in the parameters of manufacture prevents this cleaning approach, with the result that frequent complete tip replacement is required for proper STM operation, leading to high operating costs. Further, each tip replacement may require instrument recalibration due to non-homogeneity of the tips.

V. Proposed Nanotechnological Engineering of Tips

Fundamental to solution of uniformity in tip construction is uniformity of construction of the tip substrate. Known nanotechnological materials processing techniques are used to create an atomically flat substrate, and the tip can be created in an additive fashion rather than a subtractive fashion, allowing easy removal of adhered impurities and renewal to atomic sharpness.

An atomically flat substrate can be created by essentially "freezing" a material in a non-equilibrium state. If a molten metal is cooled at a rate exceeding 1 million degrees Centigrade per second, then normal formation of material dislocations and voids are severely inhibited, with the result that an atomically flat state results. Currently in commercial use, the chill-block-melt-spinning apparatus is used to create an atomically flat metal ribbon. Powdered metal is injected under pressure into a cylinder and the metal is then melted. A nozzle from the cylinder is directed upon a rapidly spinning cooled wheel and an atomized metal is then sprayed on this moving surface with the result that a thin ribbon of metal is produced substantially free of surface roughness and defects.

From the flat substrate one may then build up a conical microstructure. One method is use to create

multiple peaks, whose number may be regulated by surface masking is by laser interference metallic

deposition. As explained by G. Cau in Nanostructures and Nanomaterials and shown in Figure 4, two

laser beams are placed parallel to an atomically flat surface and perpendicular to each other, creating an

electric field interference pattern.[9] Placement of this field enhanced surface in a vapor of metal ions will

cause such ions to deposit and align according to the interference pattern leading to a highly uniform and

regular multiple tip unit. With uniform geometry and materials, the variations in manufacture are

minimized, and with multiple close tips instead of one creating the STM signal, D and P orbital patterns

uniquenesses of single peaks are minimized.
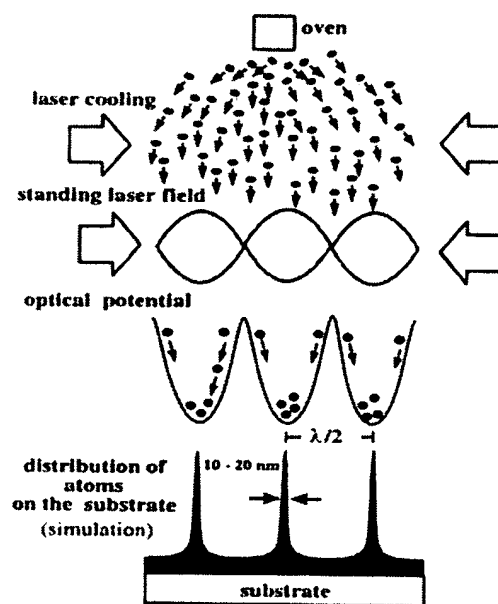
Schematic illustrating the basic principles of neutral atom lithography with light forces. [B. Brezger, Th. Schulze, U. Drodofsky, J. Stuhler, S. Nowak, T. Pfau, and J. Mlynek, *J. Vac. Sci. Technol.* B15, 2905 (1997).]

Figure 4. Neutral Atom Lithography (taken from Fig.7.7 of Reference 9, Cao)

Other methods of construction of micro cones on atomically flat surfaces can be used. For example, one

could laser drill an atomically flat mask, place such a mask over an atomically flat substrate and then

create regularly placed growth nidus by vapor deposition of metal atoms in a clean atmosphere on the

substrate through the holes. Placement of this modified planar surface in an electrolytic bath, with a second non-modified atomically flat surface facing it, and applying an electric current with the correct intensity and polarity will cause electrolytic deposition of atoms of the second surface preferentially upon the growth niduses, the locations of least electrical resistance. In this way a set of atomically sharp conal whiskers are created, in an array or arbitrary size, with uniform properties for the composite STM tip. Further, in the event that these multiple cones become contaminated during STM operation, one could use high voltage blow-off of the contaminant, as the underlying tip structure is well characterized. Even if there were some loss of sharpness in the cleaning process, one would reinsert the blunted composite tip into an electrostatic bath as noted to regrow the atomically sharp conal whiskers. Use of a 2x2 or 3x3 multiple tip matrix would also increase STM sensitivity by providing a scanned signal as the object surface protrusions are brought under sections of the tip peaks. Further, as opposed to using piezoelectric manipulation to control probe tip movement in the orthogonal x,y,z planes only, one could place such piezocrystals at oblique angles to the surface allowing angular control of the composite tip, and tracing over the descending slope of the object surface hillocks. This control may be though of as similar to the head motion of a 6-axis CNC drilling machine as opposed to the existent x,y,z 3-axis movement.

VI. Conclusion

Current methods of tip manufacture, primarily subtractive, while creating atomic sharpness necessary for STM operation, suffer from non-uniformity and lack of ability to be effectively cleaned. Constant replacement is costly, both for the actual replacement tip, and for the need for STM recalibration with each new tip. Further, single sharp tips for STM require some empirical instrument calibration as the exact geometry of the tip is not known a priori. The proposed new method of manufacture is an additive process, allowing highly uniform tip fabrication, manufacture of multiple uniform tips on a single substrate, allowing multi-tip scanning to minimize the geometry effects of a single tip, and an additive process for tip reconstitution after elimination of impurity adherents.

VII. References

1. Woodruff, D. and Delchar, T., <u>Modern Techniques of Surface Science-Second Edition</u>. Cambridge, U.K.: Press Syndicate of the University of Cambridge, 1994.

2. Frantsesson, A. and Zuev, V.: "Recent Progress in Scanning Microscopy", Journal of Russian Laser Research, Vol. 22, No. 4, 2001, pp. 295-305.

3. Tersoff, J. and Hamann, D., "Theory of the Scanning Tunneling Microscope" Physical Review B, Vol. 31, No. 2, 1985, pp. 805-813.

4. Chen, C., "Origin of Atomic Resolution on Metal Surfaces In Scanning Tunneling Microscopy", Physical Review Letters, Vol. 65, 1990, pp. 448-451.

5. Aeschimann, L., et al., "Characterization and Fabrication of Fully Metal-Coated Scanning Near Field Optical Microscopy SiO_2 Tips", Journal of microscopy, Vol. 209, Pt. 3, Mar 2003, pp.182-187.

6. Liu, C. and Gample, R.: "Mass-Producible Monolithic Silicon Probes for Scanning Probe Microscopes" Sensors and Actuators, A71, 1998, pp. 233-237.

7. Tabib-Azar, M. and Wang, Y.,"Design and Fabrication of Scanning Near-Field Microwave Probes Compatible with Atomic Force Microscopy to Image Embedded Nanostructures", IEEE Transactions on Microwave Theory and Technique, Vol. 52, No. 3, Mar 2004, pp. 971-979.

8. Cruchon-Dupeyrat, S. et. al., "Nanofabrication using Computer-Assisted Design and Automated Vector-scanning Probe Lithography" Applied Surface Science, Vol 175-176, 2001, pp. 636-642.

9. Cao, G. Nanostructures and Nanomaterials. London: Imperial College Press, 2004, pp. 290-292.

IN THE UNITED STATES PATENT AND TRADEMARK OFFICE

In re:	Robert Indech	)	Docket No:	23050-RA	
		)			
Serial No.:	10/735,406	)	Examiner:	Behrend, Harvey E.	
		)			
Filed:	December 12, 2003	)	Group Art:	3641	

For: APPARATUS AND METHOD FOR FACILITATING NUCLEAR FUSION

RESPONSE TO OFFICE ACTION OF JULY 19, 2005

EXHIBIT C

CONTACT US

Technologies | Applications | Services | Research Materials | Corporate Info | News & Publications | Contact Us

CONTACT INFORMATION

Integran Technologies Inc.
1 Meridian Road
Toronto, ON, Canada
M9W 4Z6

Tel: 416-675-6266
Fax: 416-675-1666

Request Information

Integran is located in Toronto, Canada, situated minutes away from Toronto's Pearson International Airport.

Customer Relations & General Information

For customer relations and general information regarding Integran's technologies, applications, services, news, publications and other inquiries please use our **web-form** or email **crm@integran.com**.

Research Materials

Try **ordering online**, or filling out our **web-form**.

Employment Opportunities

As a rapidly growing company, Integran is constantly looking for talented, highly motivated individuals to augment its technical and business team. As specific opportunities arise, they will be posted on this web site. However, in order to remain at the leading edge of technological innovation, Integran always welcomes applications from exceptional scientists and engineers with specific technical and business expertise in our principal lines of business, i.e., nanotechnology, interfacial materials. All applications are dealt with in the strictest confidence, and are retained on file for a period of one year. Send your application to **careers@integran.com**.
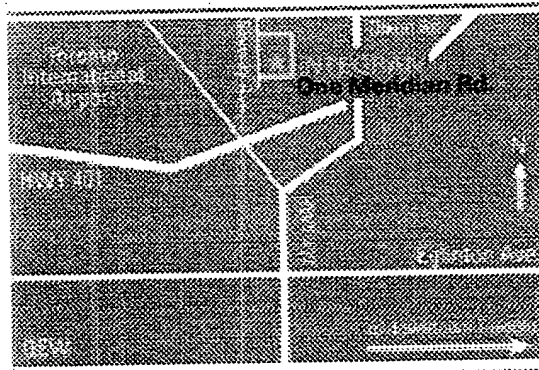
INTEGRAN

MATERIAL SALES

Technologies | Applications | Services | Research Materials | Corporate Info | News & Publications | Contact Us

Fully Dense Freestanding Metal and Alloy Foils

NANOPLATE® FOILS

RELATED INFORMATION

Other Materials:
- **Nano Coatings**
- **Nano Powders**
- **GBE® Materials**

· **Manage Order**

Nanoplate® Foils
Integran offers the world's first fully dense nanocrystalline structured metals and composite parts. Others typically achieve nanocrystalline grain sizes through consolidation of powders, inheriting the traditional drawbacks in porosity. Integran's bottom-up approach creates fully-dense parts in a single process in any form factor required. Sheet-stock of our toughest materials are now available.

Note: All prices listed in US Dollars

Nickel (99.9%)
  Attributes: ~20nm average grain size - high strength, high resilience, excellent corrosion resistance.
  Applications: Springs, MEMS, high yield sputtering targets

Item #	Sample Size in (mm)	Unit Price	Quantity Required	Manage Order
Ni-F-1A	0.002 x 1 x 1 (0.050 x 25.4 x 25.4)	$115.00	1	Add
Ni-F-1B	0.002 x 3 x 3 (0.050 x 76.2 x 76.2)	$750.00	1	Add
Ni-F-2A	0.004 x 1 x 1 (0.10 x 25.4 x 25.4)	$120.00	1	Add
Ni-F-2B	0.004 x 3 x 3 (0.10 x 76.2 x 76.2)	$800.00	1	Add
Ni-F-3A	0.006 x 1 x 1 (0.15 x 25.4 x 25.4)	$130.00	1	Add
Ni-F-3B	0.006 x 3 x 3 (0.15 x 76.2 x 76.2)	$850.00	1	Add
Ni-F-4A	0.008 x 1 x 1 (0.20 x 25.4 x 25.4)	$135.00	1	Add
Ni-F-4B	0.008 x 3 x 3 (0.20 x 76.2 x 76.2)	$900.00	1	Add
Ni-F-5A	0.02 x 1 x 1 (0.50 x 25.4 x 25.4)	$300.00	1	Add

Nickel- 20%Iron
  Attributes: ~20 nm average grain size - high strength, high resilience, excellent magnetic properties.
  Applications: Springs, electrical contacts, soft magnets

Item #	Sample Size in (mm)	Unit Price	Quantity Required	Manage Order
Ni20Fe-F-1A	0.002 x 1 x 1 (0.050 x 25.4 x 25.4)	$130.00	1	Add
Ni20Fe-F-1B	0.002 x 3 x 3 (0.050 x 76.2 x 76.2)	$850.00	1	Add
Ni20Fe-F-2A	0.004 x 1 x 1 (0.10 x 25.4 x 25.4)	$135.00	1	Add
Ni20Fe-F-2B	0.004 x 3 x 3 (0.10 x 76.2 x 76.2)	$900.00	1	Add
Ni20Fe-F-3A	0.006 x 1 x 1	$150.00		

INTEGRAN TECHNOLOGIES

NANOMATERIAL PROCESS

RELATED INFORMATION

Review Our Applications

Order Nanomaterials Now
- **Powders**
- **Coatings**
- **Foils and Plates**

Contact Us for More Info

Decreasing grain size, increasing performance; Integran's Bottom-Up Nanomaterial Process delivers unparalleled material performance in a cost effective one-step process.

Via a patent-protected electrosynthesis technology, materials having average crystal sizes 1000-times smaller than those found in conventional materials can be inexpensively produced.

Decreasing the Grain Size of Materials...
Typical metals and ceramics have crystalline structures with average grain sizes of several microns. Integran's patented bottom-up process, creates materials with 1000 times smaller grain sizes.

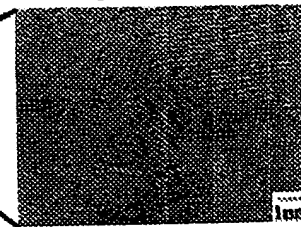**Electron micrographs illustrating the crystalline structure**

Conventional Material   Nanocrystalline Material   TEM Magnified View
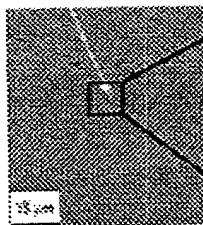
The nanocrystalline material has an average grain size of 20 nm. This is about 1000x smaller than the conventional material, at about 20 microns

...Drastically Improves Material Performance
Properties of metals are governed by the Hall-Petch relationship – as grain size decreases, strength increases. Nanocrystalline materials are characterized with significant increases in:

- Yield Strength
- Ultimate Tensile Strength
- Hardness

...Without Sacrificing Ductility
"A value of 5% elongation; often used by structural designers, is used to separate ductile from brittle behavior. To date, (Integran's) nanomaterial may be the only example of nanocrystalline material produced by a one-step process exhibiting ductility behaviour"

C.C. Koch in "Ductility in Nanostructured & Ultrafine Grained Materials: Recent Evidence for Optimism"
J. Metastable & Nanocrystalline Materials, Vol.18 (2003)pp.9-20.

Other characteristics of nanocrystalline materials include:

- Wear Resistance & Resilience
- Thermal Shock and Fatigue Resistance
- High Magnetic Saturation and Coercivity (@60Hz)
- Enhanced Anti-Microbial Activity

IN THE UNITED STATES PATENT AND TRADEMARK OFFICE

In re:	Robert Indech	)	Docket No:	23050-RA	
		)			
Serial No.:	10/735,406	)	Examiner:	Behrend, Harvey E.	
		)			
Filed:	December 12, 2003	)	Group Art:	3641	

For: APPARATUS AND METHOD FOR FACILITATING NUCLEAR FUSION

RESPONSE TO OFFICE ACTION OF JULY 19, 2005

EXHIBIT D

Nanofabrication of a two-dimensional array using laser-focused atomic deposition

R. Gupta, J. J. McClelland,[a] Z. J. Jabbour, and R. J. Celotta

Electron Physics Group, National Institute of Standards and Technology, Gaithersburg, Maryland 20899

Fabrication of a two-dimensional array of nanometer-scale chromium features on a silicon substrate by laser-focused atomic deposition is described. Features 13 ± 1 nm high and having a full-width at half maximum of 80 ± 10 nm are fabricated in a square array with lattice constant 212.78 nm, determined by the laser wavelength. The array covers an area of approximately $100\ \mu\text{m}\times200\ \mu\text{m}$. Issues associated with laser-focusing of atoms in a two-dimensional standing wave are discussed, and potential applications and improvements of the process are mentioned.

New methods for fabrication of nanometer-scale structures have been under intensive investigation recently because of the perceived benefits which might arise, such as smaller electronic devices, higher-density information storage, and novel materials. Within the past three years, a new technique for nanostructure fabrication involving laser-focused atomic deposition has been demonstrated.[1-3] In this paper we present a significant enhancement of the original technique, which was used to fabricate lines on a substrate, to demonstrate the first two-dimensional fabrication. With these new results, we also discuss some of the considerations associated with generalizing the dimensionality of the process.

In laser-focused atomic deposition, a laser light-field is used to control the motion of atoms as they deposit onto a surface. This approach has a number of potential advantages in comparison with conventional fabrication techniques, such as optical or electron-beam lithography. The advantage over optical lithography lies in the potential for much higher resolution. Optical techniques are fundamentally limited by diffraction to a minimum feature size of about half the wavelength of the light used. For ultraviolet light, this corresponds to about 100 nm. Free-flying thermal atoms, on the other hand, have De Broglie wavelengths of order 10 pm, so diffraction effects can in principle be reduced to a negligible level. The actual resolution limits of laser-focused atomic deposition are still a subject of research, though structures have already been demonstrated at the 65 nm level and theoretical predictions suggest that 5–10 nm features may be possible.[2]

This range of feature size is already just attainable with electron beam lithography;[4] however this process is inherently serial, that is, a complex pattern must be fabricated by scanning the electron beam across the surface. For large, complex patterns, the fabrication time and associated drift problems make electron beam lithography less desirable. Laser-focused atomic deposition, on the other hand, does not suffer from these limitations because it can be implemented in a parallel fashion.

A one-dimensional schematic of the two-dimensional laser-focused atomic deposition process used in the present work is shown in Fig. 1. A laser standing wave is generated across the surface of the substrate, and chromium atoms, collimated to 0.25 mrad in each of two dimensions by laser cooling,[5] are directed at the surface, traversing the laser field on their way to deposition. The laser field, produced by a single-frequency CW dye laser, is tuned 500 MHz (100 natural line widths) above the atomic resonance line in chromium at $\lambda = 425.55$ nm (vacuum wavelength). With this tuning, a dipole force[6] is exerted on the atoms toward the low intensity regions of the light field. The result is a concentration of atoms at the nodes of the standing wave, which occur at intervals of $\lambda/2 = 212.78$ nm.

In one dimension, the process as depicted in Fig. 1 is relatively straightforward. One aspect of the geometry illustrated in Fig. 1 that simplifies the implementation of this process is the fact that the positions of the deposited lines on the substrate depend only on the standing wave node positions, which in turn depend primarily on the absolute distance along the substrate from the mirror generating the standing wave. To first order, variations in the position or direction of the laser beam have no effect on the node positions, and as long as good stability is maintained between mirror and substrate, the periodicity of the pattern will be stable.
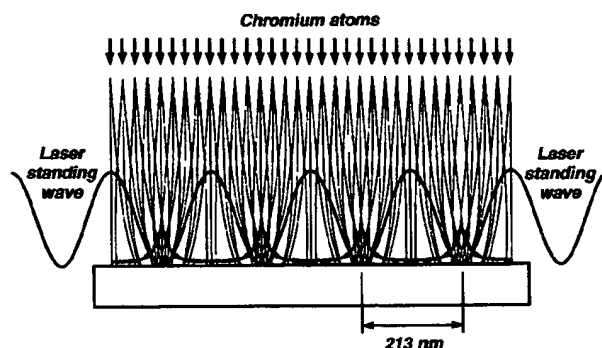

FIG. 1. One-dimensional schematic of laser-focused atomic deposition process, showing chromium atoms being focused by a laser standing wave into its nodes. The trajectories and the deposited peaks represent the results of actual calculations of the focusing process, though the relative vertical scales are highly distorted for clarity.

[a]Electronic mail: jabez@epg.nist.gov

For a two-dimensional deposition, the standing wave is formed by crossing two one-dimensional standing waves at 90° across the substrate. With this higher dimensionality, the nodes of the two-dimensional standing wave become more complex, depending on the polarizations of the constituent standing waves and also in some cases on their relative temporal phase. There are still zero points in the light intensity at locations on the surface that are an integral number of half-wavelengths from each standing wave mirror, but examination of an expression for the net electric field amplitude[7] shows that additional nodal patterns can exist, and these can shift around as the temporal phase difference between the standing waves varies.

One approach to eliminating unwanted variations in the nodal pattern due to temporal phase variations is to generate the two orthogonal standing waves in an actively-stabilized optical cavity.[8] Another approach,[9] which is useful when stability of the nodal topography is desired but absolute position is unimportant, makes use of three laser beams intersecting at 120°. For the present work we have made use of the fact that one can choose a polarization scheme in which the temporal phase does not affect the nodal pattern or position. If one chooses orthogonal linearly-polarized standing waves, with one polarized perpendicular to, and the other parallel to, the plane of the substrate, the resulting intensity distribution is given by

$$I(x,y) = 4I_0(\sin^2 kx + \sin^2 ky) \tag{1}$$

where I_0 is the intensity of a single incident wave, $k = 2\pi/\lambda$ is the wave vector of the light, and the x- and y-axes are defined to lie in the plane of the substrate. The intensity given by Eq. (1) forms a pattern of nodes and peaks on a $\lambda/2 \times \lambda/2$ square lattice with the peaks separated by saddle regions along $\hat{x}$ and $\hat{y}$ at half the intensity.

While the intensity of Eq. (1) does not suffer from temporal phase disturbances, it has potential drawbacks that could in principle cause problems with a deposition experiment, though these appear to be less severe in practice. First, it might seem that since the intensity does not have cylindrical symmetry around the potential minima, the resulting deposited spots would not be round. However, the intensity is, in fact, surprisingly symmetric in the regions near the minima. This can be seen mathematically by converting x and y to the polar coordinates (r,θ) and noting that $I(r,\theta) \approx 4I_0 k^2 r^2$ (i.e., the θ-dependence drops out) for $kr \ll 1$. Exactly how much effect the non-symmetric regions of the potential (where kr is not much less than 1) have on the deposited pattern relative to the symmetric regions is difficult to predict without a ray-tracing calculation.[10] Nevertheless, the experimental results indicate that there is little effect.

Second, it must be noted that while the intensity in this configuration does not depend on the relative temporal phase, the polarization of the electromagnetic field is complicated. In fact, the local polarization varies dramatically as a function of x and y over the scale of a wavelength, and exactly what form this variation takes depends on the relative temporal phase. The local polarization of the field can be very important because it can determine the strength of the
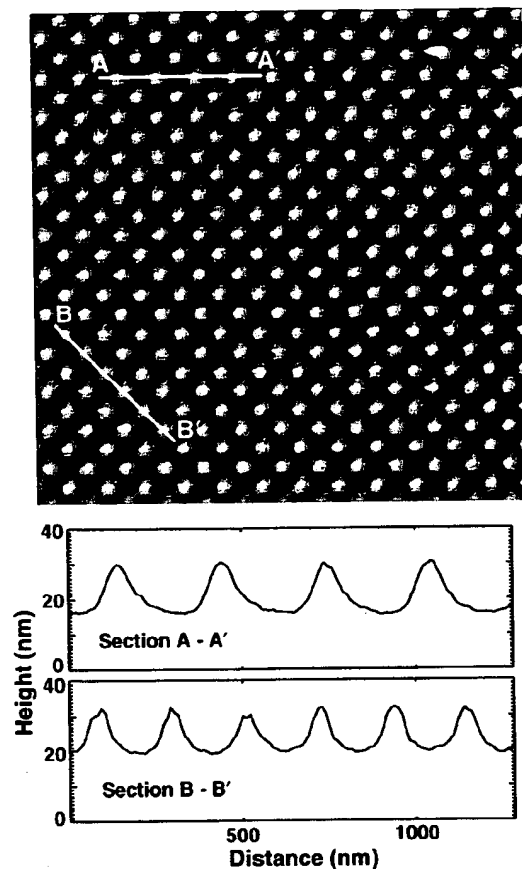

FIG. 2. Atomic force microscope (AFM) image of chromium features formed by laser-focused atomic deposition in a two-dimensional standing wave. The image covers a $4\,\mu m \times 4\,\mu m$ region of the sample. The features are on a square lattice with spacing 212.78 nm, which is determined by the laser wavelength. The standing wave is formed by superimposing two one-dimensional standing waves oriented at 45° and 135° to the figure. Also shown are two line scans, labeled A–A' and B–B', whose locations are indicated on the AFM image. The vertical scale for the line scans was determined by the AFM calibration, and the offset was estimated by requiring that the integral under the surface equal the total amount of material deposited, obtained from flux measurements.

laser-atom interaction. Chromium atoms entering the standing-wave field are in their ground state, but are distributed among a number of degenerate magnetic sublevels. The strength of the laser-atom interaction for each magnetic sublevel varies for different polarizations of the laser, due to differences in the Clebsch-Gordan coefficients for the various transitions between the different magnetic sublevels.[11] The result is a potentially wide variation in the force on the atom as a function of space, and also time if the temporal phase is not stabilized.

Despite these potential problems, it appears that a sufficiently symmetric and stable potential exists for a well-defined pattern of features to be created. Figure 2 shows an atomic force microscope (AFM) image of a 4 $\mu m \times 4$ μm region of the two-dimensional chromium pattern deposited on a silicon substrate at room temperature. For this deposition, the laser beams for the two dimensions had $1/e^2$ diameters of 0.13±0.02 mm and each contained a single-beam traveling-wave power of 12±1 mW.[12] The total deposition

time was 20 min. The full pattern covers an area of about 100 μm×200 μm, and is quite uniform across the entire area. The lattice constant of the pattern, $\lambda/2$ or 212.78 nm, was considered to be known more accurately than the horizontal calibration of the AFM, so this value was used to put the horizontal dimensions of the image on an absolute scale.

Also shown in Fig. 2 are two line scans, showing the shape of the features in two directions. These line scans have been put on a true vertical scale, including the background level, by normalizing the surface topography to the average deposition thickness of 20 nm, estimated (with an accuracy of about ± 5 nm) from previous characterizations of the deposition rate. Line scans such as the ones depicted in Fig. 2 and others taken at a variety of locations on the sample indicate that (without correction for AFM tip shape) the features are 13 ± 1 nm high, and have a full-width at half maximum of 80 ± 10 nm. The cause of the slight asymmetry in line scan A–A' is unknown, though we believe it to be an AFM artifact.

As the line scans indicate, the regions between the features are also covered with chromium. This background is a result of other isotopes in the atomic beam which are not affected by the laser light (16% of the atoms), atoms which are transferred to the metastable D-state during the optical collimation step (an estimated 7% of the atoms), and atoms that are in the high velocity tail of the Maxwell-Boltzmann velocity distribution emerging from the chromium evaporation source. Scan B–B' appears to have a slightly higher background level, arising we believe because it samples the saddle regions of the standing wave, while A–A' samples the true nodes.

Various mechanisms could be implemented to reduce the background seen in Fig. 2, if desired. For example, the undesirable isotopes and D-level atoms, as well as some of the high velocity atoms, could be removed from the beam by a laser deflection process. Alternatively, it is possible that a uniform etch of the chromium surface as deposited could remove the background before eliminating the features completely.

This work demonstrates that laser-focused atomic deposition can be successfully used to create a uniform, two-dimensional nanometer-scale pattern on a substrate. In its current form, the pattern shown in Fig. 2 could prove extremely useful as a calibration standard on the nanometer scale. The features represent essentially a "contact print" of a light wave, the wavelength of which is tuned with extremely high precision to an atomic resonance whose frequency is know with very high accuracy (about 1 ppm). Thus, within the limits of some geometrical corrections that can be kept very small (of order 10 ppm or less), the lattice spacing accuracy is extremely high.

With additional enhancements of this technique, further applications can be envisioned. Elimination or removal of the background will result in the creation of an array of isolated nanoscale metal dots on a surface. These could be used to study, e.g., transport phenomena, or quantum dot effects if fabricated on a semiconductor. Further, they could be used as an etch mask[13] to transfer the pattern to a substrate material, allowing extension of the fabrication techniques to other materials. Improvement of the resolution, which should be possible down to the 10 nm level, could lead to the possibility of scanning the substrate during deposition, creating almost any desired pattern, replicated within each unit cell of the lattice across the substrate. Furthermore, the interference of many standing waves incident from a range of angles with controlled phase could be used to generate more complex patterns.

[1] G. Timp, R. E. Behringer, D. M. Tennant, J. E. Cunningham, M. Prentiss, and K. K. Berggren, Phys. Rev. Lett. **69**, 1636 (1992).

[2] J. J. McClelland, R. E. Scholten, E. C. Palm, and R. J. Celotta, Science **262**, 877 (1993).

[3] R. E. Scholten, J. J. McClelland, E. C. Palm, A. Gavrin, and R. J. Celotta, J. Vac. Sci. Technol. B **12**, 1847 (1994).

[4] See, e.g., *Electron-beam, X-ray and Ion-beam Sub-micrometer Lithographies for Manufacturing II*, SPIE Proc. Vol. 1671, edited by M. Peckerar (SPIE, Bellingham, WA, 1992).

[5] R. E. Scholten, R. Gupta, J. J. McClelland, and R. J. Celotta (to be published).

[6] J. P. Gordon and A. Ashkin, Phys. Rev. A **21**, 1606 (1980); J. Dalibard and C. Cohen-Tannoudji, J. Opt. Soc. Am. B **2**, 1707 (1985).

[7] The net electric field can be determined by combining the four traveling waves $\mathbf{E}_{+x}=(\hat{z}E_1+\hat{y}E_2)e^{i(kx-\omega t)}$, $\mathbf{E}_{-x}=-(\hat{z}E_1+\hat{y}E_2)e^{-i(kx+\omega t)}$, $\mathbf{E}_{+y}=(\hat{z}E_3+\hat{z}E_4)e^{i(ky-\omega t+\phi)}$, $\mathbf{E}_{-y}=-(\hat{z}E_3+\hat{z}E_4)e^{-i(ky+\omega t-\phi)}$, where E_1 and E_2 are the complex electric field amplitudes determining the magnitude and polarization state of a wave traveling in the $+\hat{x}$-direction, E_3 and E_4 are the corresponding amplitudes for a wave traveling in the $+\hat{y}$-direction, and ϕ is the relative temporal phase for the two waves. See, e.g., J. D. Jackson, *Classical Electrodynamics*, 2nd ed. (Wiley, New York, 1975), pp. 273 ff.

[8] A. Hemmerich, D. Schropp, Jr., and T. W. Hänsch, Phys. Rev. A **44**, 1910 (1991).

[9] G. Grynberg, B. Lounis, P. Verkerk, J.-Y. Courtois, and C. Salomon, Phys. Rev. Lett. **70**, 2249 (1993).

[10] J. J. McClelland, J. Opt. Soc. Am. B (in press).

[11] For Cr, the variation can be as much as a factor of 28. See, e.g., V. G. Minogin and V. S. Letokhov, *Laser Light Pressure on Atoms* (Gordon and Breach, New York, 1987).

[12] Uncertainty estimates quoted in this paper are to be interpreted as one standard deviation combined random and systematic uncertainties unless otherwise indicated.

[13] N. I. Maluf, S. Y. Chou, J. P. McVittie, S. W. J. Kuan, . R. Allee, and R. F. W. Pease, J. Vac. Sci. Technol. B **7**, 1497 (1989).

IN THE UNITED STATES PATENT AND TRADEMARK OFFICE

In re:	Robert Indech	)	Docket No:	23050-RA
		)		
Serial No.:	10/735,406	)	Examiner:	Behrend, Harvey E.
		)		
Filed:	December 12, 2003	)	Group Art:	3641

For: APPARATUS AND METHOD FOR FACILITATING NUCLEAR FUSION

RESPONSE TO OFFICE ACTION OF JULY 19, 2005

EXHIBIT E

Field emission from silicon spikes with diamond coatings

V. V. Zhirnov, E. I. Givargizov, and P. S. Plekhanov
Institute of Crystallography, Russian Academy of Science, Moscow 117333, Russia

Diamond-coated silicon field emitters were fabricated and investigated. Emission currents of few μA per tip at voltages of several hundred volts were obtained from very blunt tips with curvature radii up to 3 μm. The values of the effective work function calculated from Fowler–Nordheim plot were in the range from 0.3 to 1.2 eV. Two models for an explanation of the experimental data are proposed. © *1995 American Vacuum Society.*

I. INTRODUCTION

Recent attempts in the application of diamond-coated tips as field emission sources demonstrated new emission phenomena that could be considered as very promising for vacuum microelectronic devices. There are several important advantages of diamond from the field emission point of view. (1) The negative electron affinity (NEA) of the (111) plane of diamond[1] has been suggested as the cause of observed low effective work functions obtained from a simple implementation of the Fowler–Nordheim equation. (2) The thermal conductivity of diamond is 20 W/cm °C, that is, the highest of all known materials.[2] This property is favorable for high-current applications. (3) The excellent chemical stability of the surface of diamond could enable current stability and low vacuum operation. (4) High breakdown threshold (10^7 V/cm) and rather large high-field electron velocity $(2.7\times10^7$ cm/s)^2 should enhance the maximum emission current, limited by current saturation.

The first report about growth of polycrystalline diamond particles on the very end of silicon whiskers by a hot filament chemical vapor deposition (CVD) method was presented in Ref. 3. Bias enhanced microwave plasma CVD also was used for the coating of silicon tips.[4] In Refs. 4 and 5, preliminary data of field emission from "diamond" coated silicon whiskers were presented[4,5] shortly thereafter. Emission phenomena such as high emission currents from very blunt tips,[5] large emission area, and high current stability[4] were reported.

Prospects are good for the application of diamond-coated tips for field emission devices. In this article new experimental data and results of calculation of emission parameters using various approaches are presented.

II. EXPERIMENT

A. Preparation of the tips and diamond growth

The initial tips were vapor–liquid–solid grown silicon whiskers. As-grown whiskers were of about 100 μm in height and several μm in diameter. Each whisker had a "cap" of a Au–Si eutectic alloy, a few μm in size on the very end (Fig. 1). The tips can be sharpened by wet etching and oxidation techniques and the cap is removed by sharpening (Fig. 2).

Diamond particles were grown on regular arrays of the tips by a hot filament CVD method.[3] Electron diffraction studies had shown that the particles consisted of polycrystal-

line diamond with the average size of the crystallites about 10 nm.[5] No investigations concerning band structure, defects, surface, and gap states were performed. Both as-grown samples with gold caps and sharpened ones were used in these experiments. The preferential growth of diamond at the very end of the tips, especially in the case of sharp whiskers, took place in these experiments. The possible explanation of this phenomenon was proposed in an earlier paper.[3] A regular array of silicon tips with diamond particles is shown in Fig. 3.

Depending on the preparation of the samples and the growth conditions, three kinds of tips were obtained: (1) blunt tips with a gold cap coated by a lot of diamond particles (Fig. 4); (2) sharp tips (radii of curvature from 10 to 100 nm) that had only the spherical diamond particle on the very end ("ball-on-point") (Fig. 5); and (3) sharp tips coated by a nearly continuous layer of coalescent particles of diamond ("coated point") (Fig. 6).

The samples were prepared for field emission measurements by "shaving," i.e., by carefully removing (breaking) whiskers off the substrate, leaving the only tip on each sample in order to perform experiments under well-defined conditions.

B. Field emission

The geometry used for the field emission experiments is shown in the Fig. 7. The measurements were made in an ion pumped vacuum chamber at pressures of 10^{-7}–10^{-9} Torr. The anode was a stainless steel disk 50 mm in diameter. The
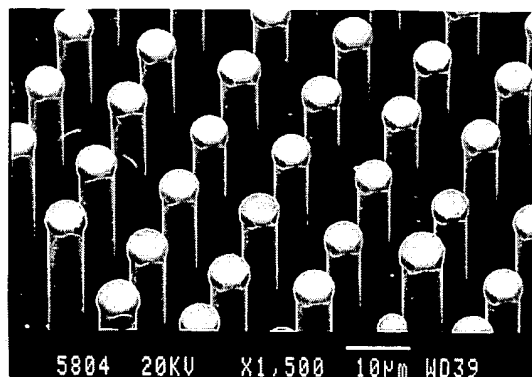

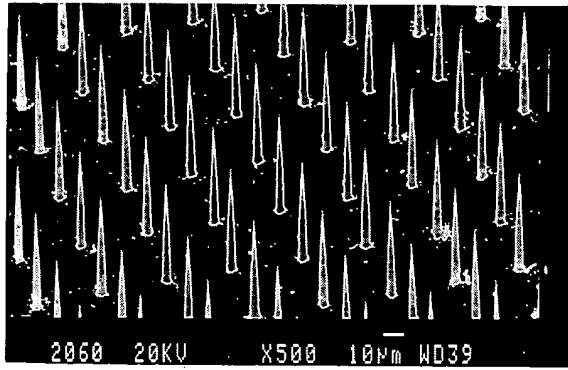FIG. 1. As-grown silicon whiskers with caps of Si–Au eutectic alloy.

FIG. 2. Sharpened silicon whiskers.

FIG. 4. The very tip of a not sharpened Si whisker with a gold cap coated by diamond particles.

spacing between the base of the sample and the anode of about double the height of the tip was maintained (see Table I).

Three kinds of field emitters were investigated (see Sec. II A, Figs. 4, 5, and 6). Current–voltage $(I-V)$ and Fowler–Nordheim (FN) plots for each of the three emitters are shown in Figs. 8(a) and 8(b).

From these experiments high emission currents (a few μA per tip) at rather low voltages (hundreds of V) were achieved from very blunt tips (up to several μm). These results were obtained on a number of samples so they can be considered as consistent among similar tips. All emission data were summarized and published elsewhere.[5]

No pressure dependence of the emission current was observed in the range of 10^{-7}–10^{-9} Torr. (A pressure of 10^{-9} Torr was achieved first by baking in the chamber; leakage of air was used to change the pressure. No analysis of partial pressures in the chamber was performed.)

III. RESULTS AND DISCUSSION

The emission parameters were obtained from FN plots by the slope-and-intersect method. The conventional field emission is described by the Fowler–Nordheim equation:

$$J=(AE^2/(\phi\ t^2(y)))\exp[-B\phi^{3/2}v(y)/E], \qquad (1)$$

where J is the current density, E the field strength at the tip, f the work function, $A=1.54\times10^{-6}$, $B=6.87\times10^7$, the func-
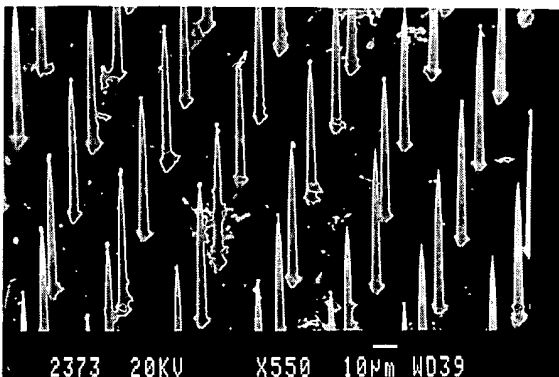
tions $t(y)$ and $v(y)$ are usually approximated by $t(y)=1.1$ and $v(y)=0.95-y$. By substituting $I=\alpha J$ and $E=\beta V$ (where α is the emitting area and β the field enhancement factor), Eq. (1) can be rewritten in the form obtained in the experiment:

$$I=aV^2\ \exp(-b/V). \qquad (2)$$

We used the point-to-plane geometry expression[6] for β in our case (see Fig. 7):

$$\beta=(h/r)(V/d). \qquad (3)$$

The tip's height h and curvature radius r were measured by scanning electron microscope (SEM) with good accuracy thus abling us to calculate β directly.

The values of the work function ϕ and effective linear dimension of the emission area α, found from FN plots, are presented in the Table I. These data are just the result of formal application of the Fowler–Nordheim equation developed for metals and for very approximate values of $t(y)$ and $v(y)$. No physical meaning could be extracted from this approach.

It should be noted that the FN constant $A=1.54\times10^{-6}$ is derived for degenerated electron gas. In general, semiconductors may have a different value of this constant, depending on carrier concentration. Since real concentration in electrons in our case is not known and the emission area, found from the FN plot depends on A, the formal calculation will

FIG. 3. Regular array of silicon whiskers with diamond particles.
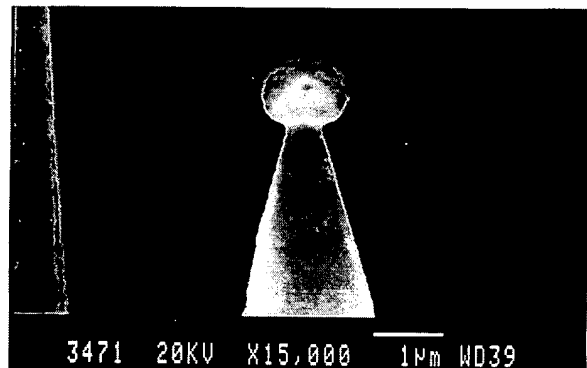

FIG. 5. Sharpened Si tips with only the diamond particle on the very ends.
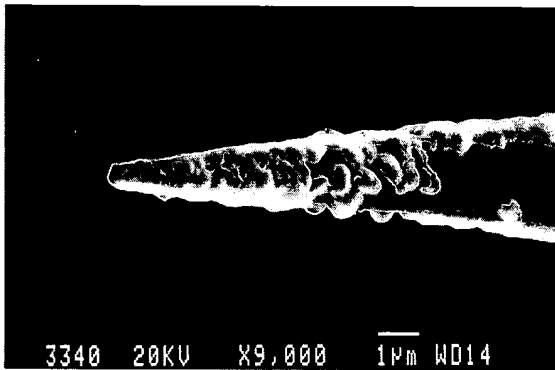
FIG. 6. Sharpened Si tips coated with a nearly continuous layer of coalescent diamond particles.

TABLE I. Experimental emission parameters of diamond-coated field emitters.

| Emitter | h (μm) | d (μm) | r (μm) | FN constants | | $\alpha^{1/2}$ (cm) | ϕ (eV) |
				a	b		
Blunt tip with coating (Fig. 4)	200	400	3	2.8×10^{-9}	8688	2.5×10^{-8}	0.37
"Ball-on-point" (Fig. 5)	100	200	0.4	3.1×10^{-9}	5372	7.9×10^{-8}	1.01
"Coated point" (Fig. 6)	200	400	0.4	3.8×10^{-9}	4146	5.7×10^{-8}	0.86

not give a real value of the emission area. However, there are several reasons why we used a "metallic" value of A.

(1) Since the diamond coatings in our experiments behaved like conductors and the saturation limit was not achieved, we assumed that the Fermi level position is near one of edges of the band gap. Further, since current saturation had not been reached in experiments. the "zero-current" approximation should be valid, i.e., the number of emitting electrons is considerably less than the number of electrons near the surface of the tip. A constant A is therefore assumed to be close its metallic value in this case.

(2) The value of $A = 1.54\times10^{-6}$ is often used for n-type Si (see, for example, Ref. 7). A comparison of emission areas before and after diamond deposition can provide useful information about the modification of emitter properties even if the change of "effective emission area" is due to a change of electron concentration. Thus, by the term "effective emission area" we mean not the real emitting part of the tip but an additional parameter for the characterization of emission behavior. A comparison of noncoated and coated Si emitters for $A = 1.54\times10^{-6}$ has been done[4] previously and the authors reported a considerable increase in the effective emission area after diamond coating.

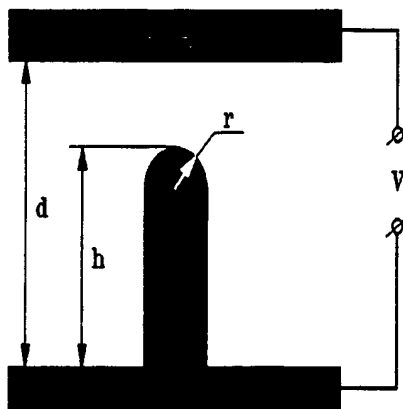In order to obtain more accurate data a "modified for a semiconductor case" FN equation was used. First, the ex-

pression for Schottky lowering of the work function barrier $y(f)$ contained a dielectric constant of material K in this case:

$$y = 3.79\times10^{-4}(E^{1/2}/\phi)(K_{s-1})/(K_{s+1}). \tag{4}$$

Second, the approximation of functions $t(y)$ and $v(y)$ in form of polynomials[7] was used.

Two different hypotheses were under consideration: (1) real lowering of the effective work function; (2) observed emission behavior not due to a low work function of blunt tips but due to the rough morphology of the tips, i.e., emission occurs from many of the very sharp microtips on the surface of the blunt tip. Then we consider both hypotheses in more detail.

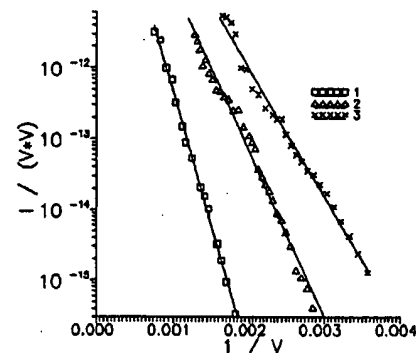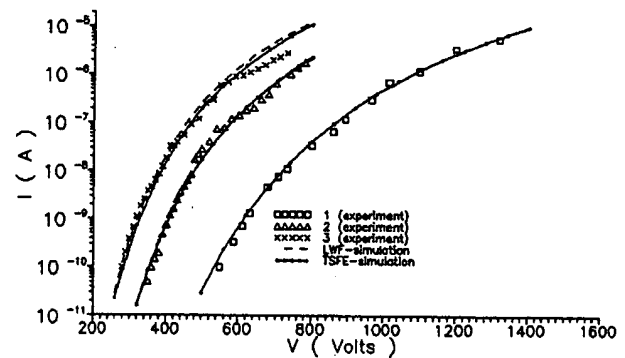*(1) Real lowering of the work function.* Assum-

FIG. 7. Geometry of the field emission experiments (values d, h, and r are given in Table I).

FIG. 8. (a) $I-V$ and (b) FN plot for three kinds of emitters: not sharpened whisker with gold cap coated with diamond particles (1), sharpened tip with only the diamond particle on the very tip (2), and sharpened tip coated with a layer of coalescent diamond particles (3). In (a) model curves, calculated using LWF and TSFE approaches are also given.

TABLE II. Emission parameters of diamond coated field emitters calculated using LWF and TSFE approaches.

	LWF approach			TSFE approach					
Emitter	h_1 (μm)	r_1 (nm)	ϕ (eV)	h_1 (μm)	r_1 (nm)	h_2 (nm)	r_2 (nm)	N	ϕ (eV)
1	200	3000	0.37	200	3000	12	0.2	200	5.4
2	100	400	1.03	100	400	8.7	0.7	10	5.4
3	200	400	0.88	200	400	9.5	0.6	10	5.4

ing the real lowering of the effective work function (low work function (LWF) model), e.g., tunneling of the electrons from the conduction band or from the surface states near the conduction band, we calculated the $I-V$ curves for $K_s=5.6$ which is known for diamond and for the geometry of the emitters used in our experiments (see Table II).

(2) Emission from small protrusions on the surface. Calculations of the emission current for this case were made on the assumption that electrons that tunnel from the valence band mainly contribute to the emission current. The value of the work function, approximately equal to the band gap of diamond, $\phi=5.4$ eV, was used in the calculations. The emitting surface may be thought of as a number of tiny tips (Fig. 9) with height of h_2 and sharpness of r_2. The minimal separation between tips s was assumed to be equal to h_2 because, if $s<h_2$, a screening effect would take place and lead to a decrease in the height of the tips. The maximum number of the tips on the surface N is thus approximately equal to
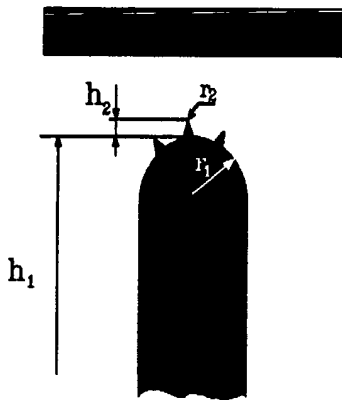

FIG. 9. Geometry of the emitter, assumed by calculations of emission from surface protrusions by using the TSFE approach.

$[(r_1/h_2)+1]$ from simple geometrical considerations for square r_1 on the side. Since no sharp surface protrusions could be seen at maximum magnification of the SEM, the h_2 should be less than 20 nm (this is the best resolution in most cases of morphological investigations by SEM).[8] The two-step field enhancement (TSFE) approach was used in this case. The electric field on the blunt tip is equal to

$$E_1=(h_1/r_1)E_0=(h_1/r_1)(V/d). \tag{3}$$

Field enhancement on the very ends of protrusions can be written as

$$E_2=(h_2/r_2)E_1=(h_1h_2/r_1r_2)(V/d). \tag{4}$$

In Fig. 8(a) $I-V$ plots calculated by these two approaches compared to experimental ones are shown. As can be seen, both models could describe experimental behavior. In the Table II emission parameters, compared to the calculated curves are presented. At present it is difficult to make a decision as to which of two approaches corresponds to experimental behavior. For the first approach it is unclear how diamond could have a number of electrons in the conduction band or near the conduction band sufficient to produce large emission currents. For the second approach an explanation is needed as to why stable ultrasharp protrusions are formed reproducibly on the diamond surface.

IV. CONCLUSIONS

Diamond-coated silicon field emitters demonstrate high emission currents at moderate voltages by very blunt tips. This behavior can be explained as due either to lowering of the effective work function or due to a large field enhancement at the tiny ultrasharp protrusions on the emitting surface.

[1]F. J. Himpsel, J. A. Knapp, J. A. Van Vechten, and D. E. Eastman, Phys. Rev. B **20**, 624 (1979).
[2]M. N. Yoder, in *Diamond and Diamond-Like Films and Coatings*, edited by R. E. Clausing *et al.* (Plenum, New York, 1991), pp. 11–16.
[3]E. I. Givargizov, V. V. Zhirnov, A. V. Kuznetsov, and P. S. Plekhanov, Mater. Lett. **18**, 61 (1993).
[4]J. Liu, V. V. Zhirnov, A. F. Myers, W. B. Choi, G. J. Wojak, J. J. Hren, S. D. Wolter, M. T. McClure, and J. T. Glass, Proceedings of the 1994 Tri-Service/NASA Cathode Workshop, Cleveland, OH, 29–31 March 1994 (unpublished), p. 99.
[5]E. I. Givargizov, Rev. Le Vide Suppl. No. **271**, 108 (1994).
[6]T. Utsumi, IEEE Trans. Electron Devices **ED-38**, 2276 (1991).
[7]K. L. Jensen and A. K. Ganguly, J. Vac. Sci. Technol. B **11**, 371 (1993).
[8]*Practical Scanning Electron Microscopy*, edited by J. I. Goldstein and H. Yakowitz (Plenum, New York, 1975).

IN THE UNITED STATES PATENT AND TRADEMARK OFFICE

In re:	Robert Indech	)	Docket No:	23050-RA
		)		
Serial No.:	10/735,406	)	Examiner:	Behrend, Harvey E.
		)		
Filed:	December 12, 2003	)	Group Art:	3641

For: APPARATUS AND METHOD FOR FACILITATING NUCLEAR FUSION

RESPONSE TO OFFICE ACTION OF JULY 19, 2005

EXHIBIT F

TIN WHISKERS: THE NEXT Y2K PROBLEM?

Engineers are racing to avert what could become a plague of short circuits in electrical and electronic devices. By Ivan Amato

THIS JUST IN

IN THE COLD VACUUM OF space, on a gleaming metal surface inside the *Galaxy 4* communications satellite, tiny whiskers of tin grew i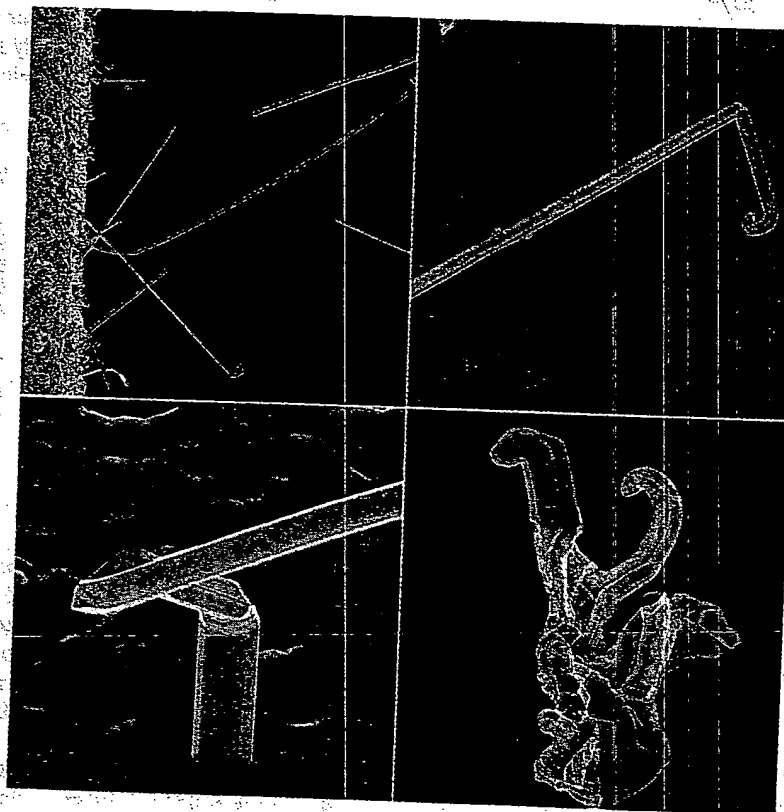n perfect stealth—until May 19, 1998, that is. That's when at least one of those whiskers bridged a pair of metal contacts in the satellite's control processor. The short circuit killed the satellite. Some 40 million pagers stopped working all over the country. Millions of dollars' worth of ATM and credit card transactions were interrupted. The $250 million satellite became, in the words of NASA engineer Henning Leidecker, "a doorstop in space."

The loss of *Galaxy 4* was just one of the more visible consequences of a little-understood problem with catastrophic potential for electronic and electrical systems: metal that grows whiskers. An F-15's radar system, pacemakers, fuse switches in air-to-air missiles, electronic relays in a nuclear power plant, and global positioning system receivers—not to mention many other satellites—all have fallen victim to the problem. One group of University of Maryland theorists has estimated that tin whiskers have caused losses of billions of dollars to date.

And the problem suddenly could be poised to get worse. The march of miniaturization means that ever smaller metal whiskers can short out the ever smaller distances between leads, solder bumps, and other jam-packed conductive surfaces in electronic systems. Furthermore, the European Union has ordered that by the middle of next year, electronic and electrical products sold in its vast market must be free of lead—and it is lead that best checks the growth of whiskers. "We are more vulnerable now than we used to be," says Ron Gedney, director-turned-consultant for the National Electronic Manufacturing Initiative (NEMI) in Herndon, Va.

The phrase "tin whiskers" is pretty darned descriptive. Under just the right lighting, if you look at a metal surface with whiskers, it sparkles. No one can tell you the specific conditions under which whiskers may or may not grow, but it usually has something to do with surface tension. Just as you might move to the less crowded outside wall of a room packed with people, metal atoms move around and reform into whiskers as a way of easing tension—even the pressing of a bracket or screw.

Until the new millennium the tin-whisker problem actually seemed like a plague of the past. The metallurgical bug first became apparent in the late 1940s to telecommunications engineers who were investigating why relays in telephone switching systems were failing. The research community came up with a whisker-quashing solution: Add 2% to 3% lead to the tin plating used in electronic assemblies, particularly on wires and leads to make them solderable. Lead-tin alloys became standards for the industry, and their use relegated tin whiskers, at least for most of us, to nuisance status.

As often happens, the solution became a problem: Lead became a material *non grata* and for good reason. It does a nasty number on neural circuitry, especially if you're a kid. To reduce human exposure to lead, governments have regulated it out of paint, gasoline, plumbing, and other sources. The relatively small amount of lead in electronic and electrical systems—about 0.2 gram in an Intel processor and about two to three grams in a motherboard—hadn't attracted much attention, but that changed as the volume of electronic waste showing up in landfills began ballooning.

Although some companies had been anticipat-

Metal whiskers grow in many shapes. The most common is the "needle" (top left).

"You don't want to go out and buy a brand-new HDTV only for it to fail before you've finished your payments."

FIRST this just In

ing an era of lead-free electronics for more than a decade and already are shipping lead-free products, the get-the-lead-out clock started ticking in earnest for the entire electronics industry in 2002 when the European Union enacted the Restriction of Hazardous Substances (RoHS) and the Waste Electrical and Electronic Equipment (WEEE) directives. Among other things, the directives mandate that by July 1, 2006, only lead-free electronic and electrical products will be legally salable in member countries. Unfortunately, no one knows for sure whether there is a no-lead substitute that will be immune to whisker growth. And that means tin whiskers and the failures they can foment could become as familiar in electronic products as flat tires are in cars.

To those who make electronic products, the no-lead restriction is akin to phasing salt out of food. Lead is a trace ingredient in these products, but its whisker-stopping and other traits have a technical taste that's hard to do without. Even though some companies are claiming to have developed reliable substitutes to lead-tin alloys, a fundamental metallurgical ignorance about why whiskers form on metals—including cadmium, zinc, and silver in addition to tin—means that there is no rock-solid basis for expecting success through any particular fix. That's why military systems are, for the moment, exempt from the lead-free requirements. But because military procurement has relied more and more on off-the-shelf consumer products, even military systems in coming years could end up with more vulnerable components.

"When you have something like lead-tin, and you have 50 years of experience with it, you hate having to change it," says NEMI's Gedney. What's too bad, he and others in the industry argue, is that going after lead in electronics is not a good way of getting a lot of environmental bang for the buck, especially when it includes the risk of bringing down more satellites. Even so, says Gedney, "no company wants to be against progress on the environmental front; every company knows it has to have a solution to this."

Some companies, such as Texas Instruments, developed lead-free technologies

**Getting the
lead out of
electronics
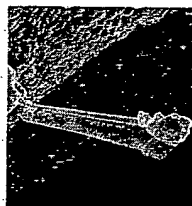may aggravate
the whisker
problem.**

even a decade ago, well before the heavy metal made it to the top of regulators' to-do lists. By the late 1990s the likelihood that lead would be excised from the diet of electronics makers and suppliers became more apparent, and in 2002 the European Union made it official. Japan, China, and several American states, including California and New Jersey, also are in various stages of outlawing lead. Denial is not an option.

Almost as out of sight to most people as the tin whiskers themselves is a worldwide network of detail-minded engineers, metallurgists, technology managers, chip manufacturers, government officials, and others who are racing against the clock to make sure that the get-the-lead-out movement does not awaken the tin-whisker dragon. They have until about right now to come up with a solution if they want to make sure that the products that ship in the coming months and years do not collectively harbor a Y2K of sorts—the wide distribution of everything from microwave ovens to missiles that are more prone to whisker-induced failure than most electronic products have been for the past half-century.

"You don't want to go out and buy a brand-new HDTV, only for it to fail before you've finished your payments," says Gedney. Researchers have come up with a variety of potential solutions. Semiconductor maker Agere Systems, for example, announced in September that it will undercoat the leads on the components it uses with nickel before it puts pure tin on top. Engineers also have developed a tin-silver-copper alloy that appears to limit whiskers to a mostly manageable fact of metallic life. However promising those lead-free solutions might look in laboratory and beta tests, however, the real assessment of their long-term ability to keep whiskering at bay will be taking place over the next few years in the wild as lead-free electronic systems are made and sold throughout the world. It's a done deal for any electronics industry player that wants to remain in the game, but all are moving forward with the nagging anxiety that they might be setting trillions of individual stages for the quiet, stealthy growth of metal whiskers that can do no good. ∎

IN THE UNITED STATES PATENT AND TRADEMARK OFFICE

In re:	Robert Indech	)	Docket No:	23050-RA
		)		
Serial No.:	10/735,406	)	Examiner:	Behrend, Harvey E.
		)		
Filed:	December 12, 2003	)	Group Art:	3641

For: APPARATUS AND METHOD FOR FACILITATING NUCLEAR FUSION

RESPONSE TO OFFICE ACTION OF JULY 19, 2005

EXHIBIT H

Physics 114 Spring 2000 Week 6.2

Muons in Matter

You just determined how the binding energy of an electron to a unit positive charge is changed by the dielectric constant of the material it's in. That problem is crucial for understanding how semiconductor devices work, Here's another problem that's important for understanding how certain types of analysis of materials work. In these techniques, particles called muons are injected into materials, and the types of sites that they bind to are studied.

A muon is like an electron but with 200 times as much mass.

(Hint- you may need to refer to the algebraic solution for the radius, etc of a hydrogen-like atom in terms of the mass, charge, ...)

a) What is the radius of the ground state of a muonic hydrogen atom, in which the muon replaces the electron? Express your answer in terms of Bohr radii. (Don't worry now about the fact that the muon mass isn't negligible compared to the proton mass.)

As we found in part a) of problem 1,

$$a \propto \frac{\hbar^2}{ke^2 m}.$$

Between the electron and the muon, the only quantity in a that differs is the mass, m. Thus,

$$\frac{a_{muon}}{a_{electron}} = \frac{m_{electron}}{m_{muon}} = \frac{1}{200}.$$

$$a_{muon} = a_{electron} / 200 = a_0 / 200$$

Note that this uses the correct value for $a_{electron} = a_0$, not $a_{electron} = 2a_0$, the value found in problem 1 using the approximation to the energy of the hydrogen atom ground state.

Also note that the advice given above not to worry about the fact that the muon mass isn't negligible compared to the proton mass refers to the fact that the m of which we speak is in fact not the mass of any single particle but rather the reduced mass of the atom. Using the reduced mass accounts for the fact that, considering the issue in classical terms, the electron does not simply orbit a stationary nucleus, but rather the electron and nucleus orbit their common center of mass. For atoms containing electrons, the reduced mass is very nearly the same as the electron mass, so we ignore this issue.

b) What is the binding energy of a muon to a proton, in eV?

As we found in part b) of problem 1,

$$E \propto \frac{k^2 e^4 m}{\hbar^2}.$$

Between the electron and the muon, the only quantity in E that differs is the mass, m. Thus,

$$\frac{E_{muon}}{E_{electron}} = \frac{m_{muon}}{m_{electron}} = \frac{200}{1}.$$

The binding energy of a particle is defined as the minimum energy that must be supplied to free the particle. All bound states of atoms have negative energy, so the muon is free as long as its energy is greater than or equal to zero. Thus, the binding energy of the muon, assuming that the muonic hydrogen is in its ground state, is the absolute value of the ground state energy.

$$E_{binding, \, muon} = |E_{muon}| = 200 \, |E_{electron}| = 200 \, |-13.6 \, eV| = \mathbf{2720 \, eV}$$

This uses the correct value for the ground state energy of the hydrogen atom, −13.6 eV, not the value found in problem 1 using the approximate expressions.

Note that when I write of the energy of the electron or muon, I really mean the energy of the hydrogen or muonic hydrogen, because as was mentioned above, not only the electron or the muon but also the proton has momentum.

IN THE UNITED STATES PATENT AND TRADEMARK OFFICE

In re:	Robert Indech	)	Docket No:	23050-RA
		)		
Serial No.:	10/735,406	)	Examiner:	Behrend, Harvey E.
		)		
Filed:	December 12, 2003	)	Group Art:	3641

For: APPARATUS AND METHOD FOR FACILITATING NUCLEAR FUSION

RESPONSE TO OFFICE ACTION OF JULY 19, 2005

EXHIBIT I

EFFECT OF SCREENING ON THERMONUCLEAR FUSION IN STELLAR AND LABORATORY PLASMAS

L. WILETS[1], B. G. GIRAUD[2], M. J. WATROUS[2], AND J. J. REHR[1]

ABSTRACT

The fusion-enhancement factor due to screening in the solar plasma is calculated. We use the finite-temperature Green's function method, and a self-consistent mean field approximation. We reduce this to one-center problems, because in the collision of two fusing ions, the turning point where tunneling may occur lies far inside the screening radius. The numerical results given by this method indicate that screening may be slightly weaker than that obtained in the most recent previous calculations.

Subject headings: elementary particles — nuclear reactions, nucleosynthesis, abundances — plasmas

1. INTRODUCTION

There remains continued interest in the solar neutrino problem, which has not been resolved in terms of the standard solar model and standard particle physics. Neutrinos are generated in thermonuclear reactions, and thermonuclear reaction rates are determined by solar physics (temperature and density), nuclear physics, and atomic shielding. The solar neutrino problem is just one of several examples where there is current interest in thermonuclear reaction rates; others include general stellar structure and laboratory plasmas. We address here the role of atomic shielding, using a finite-temperature Green's function method. Recent calculations of screening effects in the Sun have been reported by Gruzinov & Bahcall (1998), who also review previous solar screening calculations. Results of those calculations, with which we compare our present work, exhibit a scatter of 10%–30% or more in the effect of screening on fusion rates. As discussed in Gruzinov & Bahcall (1998), all of these previous calculations either are based on Salpeter's weak screening formula, which is a classical approximation, or else make unphysical approximations in order to go beyond the linear regime. Gruzinov & Bahcall attempted to rectify these limitations by including quantum effects, treating the kinetic energy in perturbation theory. Our model differs from theirs in that we do not rely on perturbation theory.

The physical model we employ is based on self-consistent Hartree plus finite-temperature local density approximation for exchange and correlation, and it assumes thermal equilibrium and adiabaticity in the internuclear coordinates. We solve this model making no further approximations or expansions, except for numerics that are carefully monitored. All previous calculations involve, e.g., expansions in the temperature, density, or quantum corrections. Carraro et al. (1988) also consider dynamic effects. Thus we believe that our approach yields results that are the most accurate to date. These results yield fusion-enhancement factors that are typically a little smaller than those recently reported (Gruzinov & Bahcall 1998).

The rate of thermonuclear fusion in plasmas is governed by barrier penetration. The barrier itself is dominated by the Coulomb repulsion of the fusing nuclei. Because the barrier potential appears in the exponent of the Gamow formula, the result is very sensitive to the effects of screening by electrons and positive ions in the plasma. Screening lowers the barrier and thus enhances the fusion rate; the greater the nuclear charges, the more important it becomes, and thus it plays an important role in the solar neutrino spectrum.

As shown below, the classical turning point radius that enters in the WKB integral for barrier penetration is very small compared with the characteristic screening lengths of interest. Inside this radius, the barrier potential is just the nucleus-nucleus Coulomb repulsion minus a constant due to screening. The constant can be interpreted simply as the difference in free energies of the system between united and separated nuclei. Since both of these are spherically symmetric, one needs only consider one-center problems.

We present here numerical calculations relevant to the solar core. The screening due to electrons in the plasma is calculated quantum mechanically by a novel Green's function method described in a recent paper (Watrous et al. 1999). The screening due to the ions is treated classically but self-consistently with the electrons. The resultant enhancement factors for several nuclear reactions are presented and compared with earlier results by other authors.

2. FUSION RATE

We work in atomic units, $e = \hbar = m_e = k_B = 1$; the unit of atomic temperature is 3.159×10^5 K. As shown by Salpeter (1954; here we follow Clayton 1968, p. 359), the fusion reaction rate between species 1 and 2 is given by

$$r_{1,2} = N_1 N_2 \int_0^\infty \psi(E) v(E) \sigma(E) dE , \qquad (1)$$

where N_1 and N_2 are the number densities of the colliding nuclides, $\psi(E)$ is the Maxwellian probability that the center-of-mass energy at large separation is E, and the cross section σ is written as a product of a penetrability factor P and a nuclear factor σ_{nuc},

$$\sigma(E) = P(E) \sigma_{\text{nuc}}(E) . \qquad (2)$$

In the WKB approximation, the s-wave penetration is given by

$$P_0(E) = \left(\frac{E_B}{E}\right)^{1/2}$$
$$\times \exp\left[-2\sqrt{2\mu} \int_R^{R_0} [Z_1 Z_2/r + U_{\text{sc}}(r) - E]^{1/2} dr \right],$$
$$(3)$$

[1] Department of Physics, Box 351560, University of Washington, Seattle, WA 98195-1560.
[2] Service de Physique Théorique, CE Saclay, F-91191 Gif-sur-Yvette, France.

with E_B the height of the barrier, μ the reduced mass, and $U_{sc}(r) < 0$ the screening potential; R is the "touching" radius (the top of the barrier), and R_0 is the classical turning radius. The integrand in equation (1) peaks at some characteristic energy E_0. For the solar interior, the corresponding classical turning radius $R_0 \approx Z_1 Z_2/E_0$, is ~ 0.005 AU, compared with a screening radius of ~ 0.5 AU. For this reason, the screening potential can be taken as a constant $U_0 \equiv U_{sc}(r = 0) < 0$ within the turning radius, acting as an effective shift in the energy:

$$r_{1,2} = N_1 N_2 \int_0^\infty \psi(E) v(E) P(E - U_0) \sigma_{nuc}(E - U_0) dE \quad (4)$$

$$r_{1,2} \propto \int_0^\infty E^{1/2} e^{-E/T} P(E - U_0) \sigma_{nuc}(E - U_0) dE \quad (5)$$

$$= \int_{-U_0}^\infty (E' + U_0)^{1/2} e^{-(E' + U_0)/T} P(E') \sigma_{nuc}(E') dE' \ . \quad (6)$$

Then, neglecting U_0 in the limit of integration,

$$r_{1,2} \approx e^{-U_0/T} N_1 N_2 \int_0^\infty \psi(E) v(E) \sigma(E) dE \ . \quad (7)$$

Screening thus enhances the reaction rate by the factor

$$f = e^{-U_0/T} , \quad (8)$$

where U_0 is given by equation (10) below. Since $U_0 < 0$, $f > 1$, corresponding to enhancement.

3. FREE ENERGY AND THE ONE-CENTER PROBLEM

The screening potential is just the change, brought about by the approaching ions, in the Helmholtz free energy

$$F = U_{internal} - TS , \quad (9)$$

as a function of nuclear separation. Because of the smallness of the turning radius, it is sufficient to consider the one-center problems and identify

$$U_0 = F(Z_1 + Z_2) - F(Z_1) - F(Z_2) \ . \quad (10)$$

What we mean here by one-center problems are the calculations of F when either charges Z_1, Z_2, or both lie at the center of the plasma. In § 4 we calculate $F(Z)$ explicitly for an independent particle model approximation, akin to the temperature dependent Hartree-Fock method. However, the free energy has a simple and completely general (for the problem at hand) interpretation, which does not depend on the mean field approximation. It is, by definition, the work required at a given temperature to introduce the nuclear charge into the plasma. The nucleus interacts with the plasma only electrostatically, so $dF = \phi(Z', r = 0) dZ'$, and thus the work required to assemble the charge Z at, say, $r = 0$ is

$$F(Z) = \int_0^Z \phi(Z', r = 0) dZ' , \quad (11)$$

where $\phi(Z', r)$ is the electrostatic potential generated in the plasma due to a nuclear charge Z',

$$\phi(Z', r = 0) = 4\pi \int_0^\infty r' dr' \left[\sum_I \rho_I(r', T) - \rho_e(r', T) \right] . \quad (12)$$

Here $\rho_e(r, T)$ and $\rho_I(r, T)$ denote the finite-temperature number density (recall $e = 1$) of the electrons and various background ions charge densities, respectively.

The one-center screening problem is solved by the methods described by Watrous et al. (1999) for the electrons

with a Kohn-Sham formalism, using the finite-temperature local density approximation (Mermin 1965) for exchange and correlation. Screening due to ions is included as well as that due to electrons. The ions are treated classically according to the Debye-Huckel method. Thus the electric potential generated by electrons and ions becomes

$$\Phi(r) = \frac{Z}{r} + \int d^3r' \frac{\sum_I \rho_I(r', T) - \rho_e(r', T)}{|r - r'|} . \quad (13)$$

The second term is the function denoted by $\phi(Z, r)$ above. Each ion density is given by

$$\rho_I(r, T) = \rho_I(\infty) e^{-Z_I \Phi(r)/T} \ . \quad (14)$$

Since $\Phi(r)$ is positive, ions are pushed outward and electrons are drawn toward the nucleus. For notational simplicity in the following, the temperature dependence of the densities will be understood and not specified explicitly.

4. ALTERNATIVE MEAN FIELD DERIVATION OF THE FREE ENERGY

We now demonstrate the equivalence of the F defined by equations (9) and (11) in the finite-temperature Hartree-Fock approximation, which is similar to the finite-temperature local density approximation actually used in our numerical calculations. In a transparent, short notation, we describe the system by a second-quantized Hamiltonian $\mathcal{H}$ containing the kinetic energy operators t_i of the particles present in the plasma, their two-body interactions v_{ij}, and the additional one-body operators $w_i = -Z/r_i$ or $+Z_I Z/r_i$ representing the contributions of the additional nuclear charge Z at the center. The temperature T enters the formalism via the usual Boltzmann factor $\exp(-\beta \mathcal{H})$, where $\beta = 1/T$. Actually, because the average electronic density and background positive charge density are fixed parameters of the problem, $\mathcal{H}$ must be replaced by the usual constrained Hamiltonian. This will read, in a short notation, $\mathcal{H} - \mu' \mathcal{N}$. Here μ' is a several-component chemical potential because of the several components in the plasma (i.e., electrons and various background ions). Accordingly the particle number operator $\mathcal{N}$ must be understood as a several-component operator. For simplicity, however, the following equations deal with the electrons only. This is because the positive ions in the background may consist of bosons as well as fermions, and we want to spare the reader the cumbersome symmetrization or antisymmetrization formulae for such backgrounds. In any case, the present paper describes the background density classically, and this density is not high enough to demand exchange terms.

The independent particle *Ansatz* approximates the eigenstates of $\mathcal{H} - \mu' \mathcal{N}$ by antisymmetrized products of single particle states (orbitals) $|i\rangle$, with an approximate spectrum made of sums of independent particle levels η_i. The infinite set of orbitals $|i\rangle$ and eigenvalues η_i defines a one-body operator $\mathcal{H}_0 - \mu' \mathcal{N}$, presumed optimal from the point of view of a variational principle: i.e., stationarity of the grand potential or free energy F.

In second quantization, the many-body density matrix used as a *trial* density operator (noted in the following by quantities carrying a subscript t) is

$$D_t = \frac{\exp\left[-\beta(\mathcal{H}_0 - \mu' \mathcal{N})\right]}{Z_t} = \frac{\exp\left(-\beta \sum_i \eta_i c_i^\dagger c_i\right)}{Z_t} , \quad (15)$$

TABLE 1

RESULTS OF SOLAR SCREENING CALCULATIONS FOR
VARIOUS VALUES OF Z

Z	$\phi(Z, r = 0)$	$\rho_e(Z, r = 0)$	$F(Z)$
1......	-2.007	2.791	-1.008
2......	-3.944	6.829	-4.009
3......	...	...	-8.962
4......	-7.884	20.76	-15.82
5......	...	...	-24.54
6......	-12.00	49.77	-35.14
7......	...	...	-47.65
8......	-16.51	108.6	-62.19

NOTE.—ϕ and ρ_e are calculated values; the free
energy F is based on the polynomial fit.

where $c_i^\dagger$ and c_i are the usual fermionic creation and anni-hilihation operators for orbital $|i\rangle$. For electrons the nor-malization denominator Z_t is

$$Z_t = \prod_i [1 + \exp(-\beta\eta_i)] , \qquad (16)$$

so the trial density becomes

$$D_t = \prod_i \frac{\exp(-\beta\eta_i c_i^\dagger c_i)}{1 + \exp(-\beta\eta_i)} . \qquad (17)$$

The *true* density matrix $D = \exp[-\beta(\mathcal{H} - \mu'\mathcal{N})]/$ Tr $\exp[-\beta(\mathcal{H} - \mu'\mathcal{N})]$, minimizes the *true* grand poten-tial, $\Omega = \text{Tr } D(\mathcal{H} - \mu'\mathcal{N} + \beta^{-1}\ln D)$. However, with an independent particle approximation, one must be content with minimizing

$$F = \text{Tr } D_t(\mathcal{H} - \mu'\mathcal{N} + \beta^{-1}\ln D_t) . \qquad (18)$$

It is easy to show that

$$\text{Tr } D_t c_i^\dagger c_i c_j^\dagger c_j = f_i f_j, \text{ if } i \neq j , \qquad (19)$$

where the Fermi occupation numbers are $f_i \equiv \text{Tr } D_t c_i^\dagger c_i = 1/[1 + \exp(\beta\eta_i)]$. Furthermore

$$\text{Tr } D_t \{-\beta\eta_i c_i^\dagger c_i - \ln[1 + \exp(-\beta\eta_i)]\}$$
$$= f_i \ln f_i + (1 - f_i)\ln(1 - f_i) . \qquad (20)$$

Finally, because $\mathcal{H} = (\mathcal{T} + \mathcal{W}) + \mathcal{V}$ is the sum of a one-body operator $\mathcal{T} + \mathcal{W} \equiv \sum_i t_i + \sum_i w_i$ and a two-body operator $\mathcal{V} \equiv \sum_{i>j} v_{ij}$, we obtain

$$F = \sum_i f_i \langle i|(t + w - \mu')|i\rangle + \frac{1}{2}\sum_{i,j} f_i f_j \langle ij|\tilde{v}|ij\rangle$$
$$+ \beta^{-1}\sum_i [f_i \ln f_i + (1 - f_i)\ln(1 - f_i)] . \qquad (21)$$

Here the tilde $\tilde{v}$ means that the matrix element $\langle ij|\tilde{v}|ij\rangle$ is antisymmetrized.

The functional derivative of F with respect to $\langle i|$ is then

$$\frac{\delta F}{\delta\langle i|} = f_i\left(t + w - \mu' + \sum_j f_j \langle j|\tilde{v}|ij\rangle\right), \qquad (22)$$

where one recognizes the action of a mean field potential, including both direct and exchange terms

$$\mathcal{U}|i\rangle \equiv \sum_j f_j \langle j|\tilde{v}|ij\rangle . \qquad (23)$$

Stationarity of F with respect to $|i\rangle$ then gives the "finite-temperature Hartree-Fock" equations,

$$(t + w - \mu' + \mathcal{U})|i\rangle = \eta_i|i\rangle, \forall i , \qquad (24)$$

where one recognizes that η_i is the Lagrange multiplier for the normalization of the orbital.

In the same way, the derivative of F with respect to η_i, or as well f_i, yields

$$\frac{\partial F}{\partial f_i} = \eta_i + \beta^{-1}\ln[f_i/1 - f_i] , \qquad (25)$$

which vanishes [see eq. (20)]. It can thus be concluded that

$$F = -\beta^{-1}\ln Z_t - \text{Tr} D_t \mathcal{V} , \qquad (26)$$

(which *differs* from $-\beta^{-1}\ln Z_t$) is stationary with respect to variations of D_t. Therefore, since $\mathcal{W}$ is proportional to the additional charge Z at the center, the derivative of F with respect to Z must be given by

$$\frac{\partial F}{\partial Z} = \text{Tr } D_t \frac{\mathcal{W}}{Z} . \qquad (27)$$

Notice also that $\mathcal{W}$ is a local potential. Hence, in the coor-dinate representation, only the diagonal part of D_t (the clas-sical density) is needed to calculate $\partial F/\partial Z$,

$$\frac{\partial F}{\partial Z} = 4\pi \int r' dr' [\rho_p(r') - \rho_e(r')] , \qquad (28)$$

which is the differential form of equations (11–12). Here $\rho_e(r')$ and $\rho_p(r')$ are diagonal matrix elements $\langle r'|D_t|r'\rangle$ in the electron and positive background sectors, respectively. It will be noticed that equation (28) gives the background density as well as the electronic density, while the preceding equations, equations (15)–(27), accounted for the electrons only. In view of the simplicity of the result due to the elec-trons, this reinstatement of the background contribution is trivial. Notice also that for the one-center problem, D_t is rotationally invariant, hence no vector label r' is needed.

The result, equation (28) is simply a reformulation of equations (11)–(12). The method of Matsubara poles used by Watrous et al. (1999) via the finite-temperature, one-body Green's function, is perfectly suited to this local calcu-lation of the density and avoids an explicit solution of equation (24). Indeed, as discussed in detail by Watrous et al. (1999), a local density such as $\rho_e(r')$ can be directly derived from diagonal matrix elements $\langle r'|(\eta - t - w - \mu' - \mathcal{U})^{-1}|r'\rangle$ of the one-body Green's function. Such matrix elements are integrated on a suitable contour in the η-complex plane. Once $\partial F/\partial Z$ is known for all values of Z smaller than $Z_1 + Z_2$, trivial integrals provide the screening U_0 according to equation (10).

5. NUMERICAL RESULTS FOR THE SOLAR CORE

Shielding calculations have been performed for $Z = 1, 2, 4, 6, 8$ at a density and temperature relevant to energy and neutrino production in the Sun. From these calculations the fusion-enhancement factors are calculated and compared with the results of other researchers. Ricci et al. (1995) have shown that enhancement factors for the relevant fusion reactions are insensitive to the location within the solar

TABLE 2

Fusion-Enhancement Factors for the Solar Interior (This Work), Compared with Other Screening Calculations

Reaction	This Work	WES	Mit	GDGC	CSK	GB
$p + p$	1.043	1.049	1.045	1.049	1.038	1.053
He + He	1.181	1.213	1.176	1.115	1.158	1.224
Be + p	1.183	1.213	1.171	1.112	1.169	1.166
N + p	1.356	1.402	1.293	1.191	1.324	1.393

Note.—WES is Salpeter's weak screening approximation (Salpeter 1954); Mit is Mitler's Thomas-Fermi–like model (Mitler 1977); GDGC is from Graboske et al. 1973; CSK is the dynamic screening model of Carraro et al. 1988; GB is from Gruzinov & Bahcall 1998.

core. We use here the set of parameters similar to those employed by Bahcall & Pinsonneault (1995), corresponding to $R/R_\odot = 0.06$. In atomic units, they are $T = 47$, $n_e = 7.63$, $X = 0.432$, $Y = 0.568$. The results are displayed in Table 1 for $\phi(Z, r = 0)$ and $\Delta\rho_e(Z, r = 0) = \rho_e(Z, r = 0) - n_e$. These quantities for other Z-values can be obtained by interpolation. $\phi(Z, r = 0)$ was fitted to a fourth-order polynomial,

$$\phi(Z, r = 0) \approx -\sum_{n=1}^{4} c_n Z^n \,. \qquad (29)$$

The integral of this quantity then yields the free energy,

$$F(Z) \approx -\sum_{n=1}^{4} c_n Z^{n+1}/(n + 1) \,, \qquad (30)$$

with $c_1 = 2.0275$, $c_2 = -0.03661$, $c_3 = 0.00594$, $c_4 = -0.000103$. Note that $\phi(Z, r = 0)$ is nearly linear in Z.

Table 2 gives the fusion-enhancement factors for several reactions of interest in the solar neutrino problem. The deviation from unity is a result of shielding. Note that the various calculations exhibit a scatter of 10%–30% and more in the deviation from unity. Although our factors are rather close to the recent calculations of Gruzinov & Bahcall (1998), they are usually somewhat lower.

6. SUMMARY AND CONCLUSIONS

The finite-temperature Green's function method of Watrous et al. (1999) has been applied to the problem of screening of the nucleus-nucleus interaction in the solar plasma. The method is based on a self-consistent, finite-temperature Kohn-Sham formalism with the local density approximation for exchange and correlation. Atomic bound states are included on an equal footing with continuum states. Fusion-enhancement factors (over pure Coulomb) are calculated for various relevant nuclear reactions at mean conditions (temperature and density) of the solar core. Comparisons with several other calculations are presented.

The method appears to have no restriction with respect to temperature or density for stars in "noncatastrophic," thermal equilibrium states. When implementing calculations for other systems, one may need to extend the range of parameters for the local exchange-correlation term, which is quite small for our solar system.

REFERENCES

Bahcall, J. N., & Pinsonneault, M. H. 1995, Rev. Mod. Phys., 67, 781
Carraro, C., Schäfer, A., & Koonin, S. E. 1988, ApJ, 331, 565
Clayton, D. D. 1968, Principles of Stellar Evolution and Nucleosynthesis (New York: McGraw-Hill)
Graboske, H. C., DeWitt, H. E., Grossman, A. S., & Cooper, M. S. 1973, ApJ, 181, 457
Gruzinov, A. V., & Bahcall, J. N. 1998, ApJ, 504, 996
Mermin, N. D. 1965, Phys. Rev. A, 137, 144
Mitler, H. E. 1977, ApJ, 212, 513
Ricci, B., Degl'Innocenti, S., & Fiorentini, G. 1995, Phys. Rev. C, 52, 1095
Salpeter, E. E. 1954, Australian J. Phys., 7, 373
Watrous, M. J., Wilets, L., & Rehr, J. J. 1999, Phys. Rev. E, 59, 3554